

3D Printable Rebar Free Concrete Members

A Technical Report submitted to the Department of Engineering Systems and Environment

Presented to the Faculty of the School of Engineering and Applied Science
University of Virginia • Charlottesville, Virginia

In Partial Fulfillment of the Requirements for the Degree
Bachelor of Science, School of Engineering

Justine Schulte
Spring, 2021.

Technical Project Team Members
Dillon Melerine
Justine Schulte

On my honor as a University Student, I have neither given nor received
unauthorized aid on this assignment as defined by the Honor Guidelines for
Thesis-Related Assignments

Signature  Date 5/13/2021
Justine Schulte

Approved _____ Date _____
Osman Ozbulut, Department of Engineering Systems and Environment

Introduction

Additive manufacturing refers to the layer-wise fabrication of a component using input from a CAD model. This technology is gaining popularity in a number of industries, like medical and aerospace, where personalized and complex products are especially advantageous. Likewise, additive manufacturing (AM) is slowly beginning to be applied in the structural engineering and architectural worlds, with several companies beginning to explore 3D printing of concrete to create full scale structures (O’Neal, 2016; Starr, 2016). Concrete can be printed via the extrusion of the cementitious materials through a nozzle and deposited in a preloaded pattern. The nozzle is then raised and the next layer is printed, repeating the process until the structure is complete. AM concrete construction offers distinct advantages over more traditional manufacturing methods, by eliminating the cost associated with formwork (which accounts for 40 - 60% of the cost of concrete cast in place constructions (Lab, 2007)), improving human safety (allowing for the automation of dangerous jobs typically performed by concrete workers (Bhardwaj et al., 2019)) and allowing for the fabrication of more complex structural members.

Conversely, with AM structures beginning to be fabricated, several challenges inherent to the AM process are emerging. One challenge is the method of reinforcement. Concrete is by nature a very brittle material that performs well in compression, but provides little tensile strength. For these reasons, steel rebar is typically placed within concrete to provide reinforcement and carry some tensile load. However, traditional rebar reinforcement isn’t easily incorporated into additive manufacturing methods, as it involves the pouring of wet concrete around pre-placed rebar. Several alternatives are being considered as potential replacements for traditional rebar reinforcement. 3D printed concrete can be reinforced by leaving gaps in the structure during deposition, so that rebar can be placed after the printing process is complete (Lu et al., 2019). However, this method limits both the possible complexity of the final geometry and the automation of the process, as additional post-printing work is needed (Soltan & Li, 2018). Another proposed solution is the use of fibers to improve the tensile capacity of the concrete (Lu et al., 2019). These mixtures, known as fiber-reinforced cementitious composite, show promise with various studies finding improved mechanical properties of concrete 3D printed with fibers (Hambach & Volkmer, 2017; Soltan & Li, 2018; Zhu et al., 2019).

Another challenge associated with AM processes optimization of printing parameters. Additive manufacturing has been found to be a highly directional process - with mechanical properties varying depending on the path with which the piece is printed. The optimization of printing parameters can open the door to the printing of more advanced structures with optimized geometries with superior properties. Such future geometries can utilize weight relief principals to support more loads by changing the distribution of material to match the forces experienced in different locations. The goal of this capstone is to couple the technique of fiber reinforcement with an optimized printing process to 3D print a concrete rebar-free beam that has a higher flexural strength than traditional unreinforced concrete. The original scope of this project included the fabrication of an optimized weight relief structure, but, due to complications in the printing process and time constraints, this aspect of the project was not completed. However, the computational side of the topic is still discussed to inform future work.

Scope

The goal of this project will be achieved through the completion of three major phases: Mixture Design, Rheology Testing Matrix and Admixture Optimization, and Mechanical Testing, outlined in Fig. 1. The project will conclude with the printing and mechanical testing of beams with different tool paths. The mechanical properties of these beams will be compared to those of fabricated by traditional cast-in-place methods to evaluate any potential increases in the flexural strength added by the AM process. Furthermore, the geometry optimization of printed beams will be discussed at the end and connected to future work.

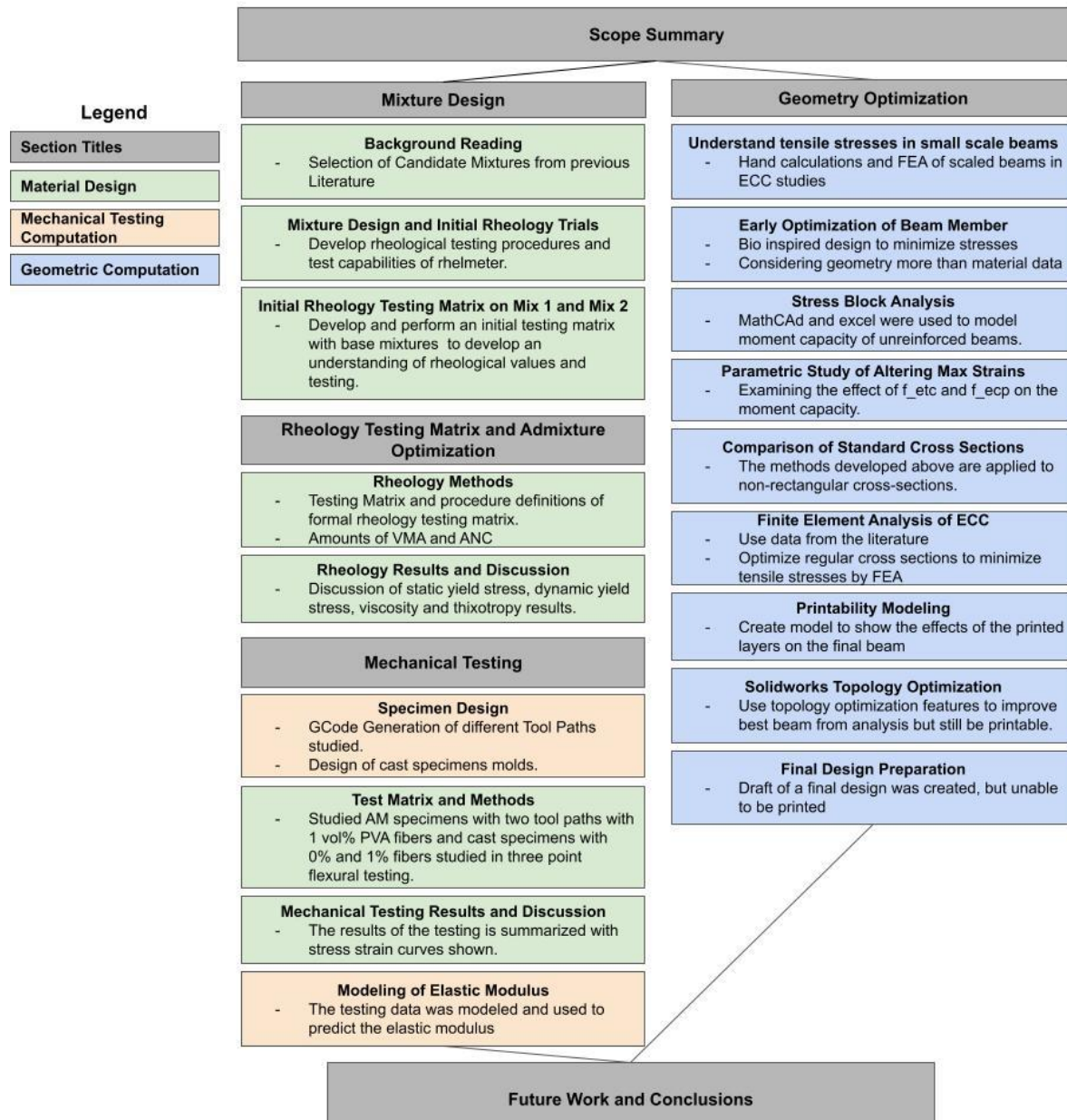


Figure 1: Summary Graphic of General Scope of the project.

Schedule

The original project schedule is given in Table 1, which depicts a critical path method (CPM) approach to outlining the schedule. Fig. 2, shows a graphical representation of the sequence of the various tasks to show how various required tasks relate to each other. This schedule was adapted as the project changed in scope and delays due to Covid were experienced.

Table 1: Schedule Overview, CPM

Activity	Description	Time (days)	EST	EFT	LST	LFT	Slack	Criticality
A	Preliminary Research/ Background Gathering	45	0	45	0	45	0	*
B	Final Testing Matrix	14	45	59	45	59	0	*
C	Beam Comparisons with Prior studies/ built examples	50	7	57	9	59	2	
D	Rheology Testing + Analysis	80	59	139	59	139	0	*
E	Printability/ Buildability Testing	40	139	179	139	179	0	*
F	Final Beam Printing	14	139	153	179	193	40	
G	Beam Topology Optimization	35	57	92	59	94	2	
H	Beam Design for Production	30	92	122	94	124	2	
I	Beam Curing	28	153	181	193	221	40	
J	Final Mechanical testing	21	188	209	221	242	33	
K	Test Data Assimilation	7	181	188	193	200	12	
L	Final Literature Review	14	122	136	124	138	2	
M	Report Writing	21	188	209	200	221	12	

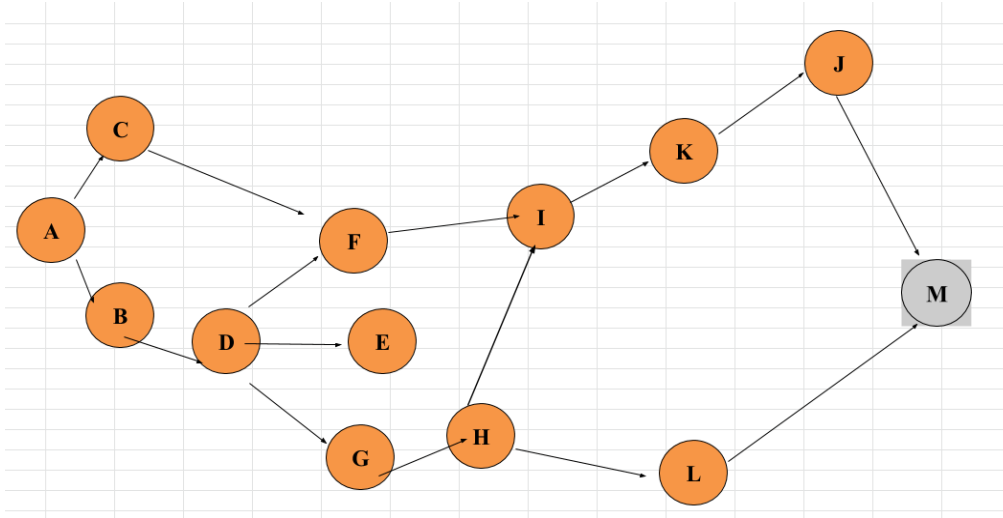


Figure 2: Activity on Node Diagram Illustrating Relatedness of Tasks in Table 1

Mixture Design

Background Reading

The first phase of the mixture design was centered on the background reading of research articles detailing the 3D printing of fiber reinforced cementitious composites to identify several candidate base mixture designs, which will undergo trial rheology testing. Based on the results of these initial trials, a mixture will be selected as the base for the material used in the fiber reinforced concrete. It is necessary to fully examine the fresh properties, because a 3D printable cement must have very specific materials properties. The mixture must have a static yield stress that is low enough to be extruded through a nozzle, yet high enough to hold its shape once deposited. This issue is further complicated by the addition of fibers, which will also ultimately affect the rheological properties. In addition to trial mixture selection, the initial rheology testing protocol was also determined during the background reading phase. Different loading protocols from the literature were evaluated and a simple stress growth shear vane test was selected for the initial testing. A stress growth test involves submerging a shear vane into a concrete mixture and rotating the vane at a constant shear rate. The resulting stress is then measured to determine the static yield stress (Ivanova & Mechtcherine, 2020). These initial stress growth tests will be later supplemented with more complex testing protocols, in order to gain a more complete understanding of the rheology.

Mixture Design and Initial Rheology Trials

Based on the available materials and the desired performance, several candidate mixtures were identified from the literature, Table 2. Mix 1 was based on a mixture used by Zhu et. al. (Zhu et al., 2019) that used polyethylene fibers to increase the tensile capacity of a concrete beam. Mix 2 was similar to mix 1, but with 15% of the fly ash replaced with silica fume. This adjustment created a larger variation in particle size with the intended result being an increase in strength. Mix 3 was based off of PVA fiber reinforced trial designs used in Soltan and Li's study (Soltan & Li, 2018). The superplasticizer (SP) and viscosity

modifying admixture (VMA) were varied in the initial rheology trials in order to gain an understanding of how they affect the static yield stress. These are two important ingredients when considering printability of concrete, as SP and VMA are expected to decrease and increase the viscosity respectively. These initial tests were completed with no reinforcement fiber added. The purpose of these trials is to look purely at the behavior of the base mixtures.

Table 2: Base Mixture Designs based on previous studies. All components are reported in ratios with respect to the total weight of binders (Cement, Cement Type III, Fly Ash and Silica Fume).

Trial Mixtures	Silica Sand	Cement Type I/II	Cement Type III	Fly Ash	Silica Fume	Water
Mix 1	.4	.4	.03	.57	0	.28
Mix 2	.4	.4	.03	.42	.16	.28
Mix 3	.39	.6	.07	.19	.13	.37

The first mixture studied was Mix 1. The mixture was created by mixing the dry binder materials together in a planetary type mixer before adding the SP, VMA and water to the mixture. Finally, the silica sand was added to the concrete. Four different versions of this mix design were tested with different amounts of SP and VMA - .2% SP, 1% SP, .5% SP and .5% SP + .3% VMA. These amounts were selected based on the manufacturer recommendation for dosage and the results of prior tests. After each mixture was fully mixed, the mixtures were visually inspected to assess the probability that they would be printable. Finally, a stress growth shear vane test was completed using an Anton Paar Physica MCR 301 Rheometer. The test applied a constant strain rate of .1/s for 3 minutes - the 3 minutes time span allowed for the measurement of any potential growth in stress over time.

The results of Mix 1 rheology tests are summarized in Fig. 3. The first test conducted used .2% SP and no VMA, which resulted in a mixture that appeared to be printable. However, when the rheology test was performed the shear stress values obtained extended beyond the measuring capabilities of the rheometer and thus no static yield stress value was recorded. In order to obtain a lower viscosity, the next test used 1% SP and no VMA. This resulted in an unprintable, extremely runny mixture with very low shear stresses that is not suitable for printing. The next batch lowered the SP amount to .5%, which resulted in a mixture that was still very low in viscosity. The final variation of Mix 1, used the .5% SP and added .3% VMA. This resulted in a mixture that had a relatively high stress capacity, but did not max out the rheometer. Even though it was not printable, 5%SP and .3% VMA was determined to be the best combination tested.

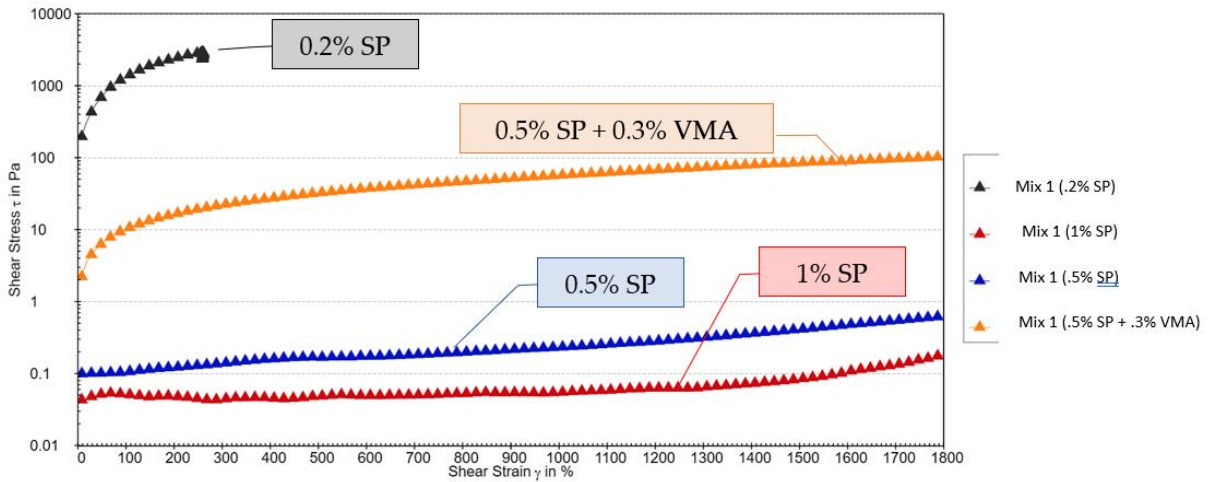


Figure 3: Shear stress and strain graph showing the effects of various amounts of SP and VMA on the base mix 1.

The other two base mixtures, mix 2 and 3, were prepared and tested using the same procedures. Based on the testing of Mix 1, the amounts of SP and VMA used were .5% and .3% respectively. This was done to allow for comparison between the base mixtures. The results of the rest of trials are shown in Fig. 4. From the graph, it can be seen that the base Mix 3 had the highest viscosity, followed by Mix 2 and then Mix 1. However, it should be noted that none of the mixtures appeared to be printable. However, the addition of fibers to the mixtures may increase the static yield stress, so that the mixtures will be printable.

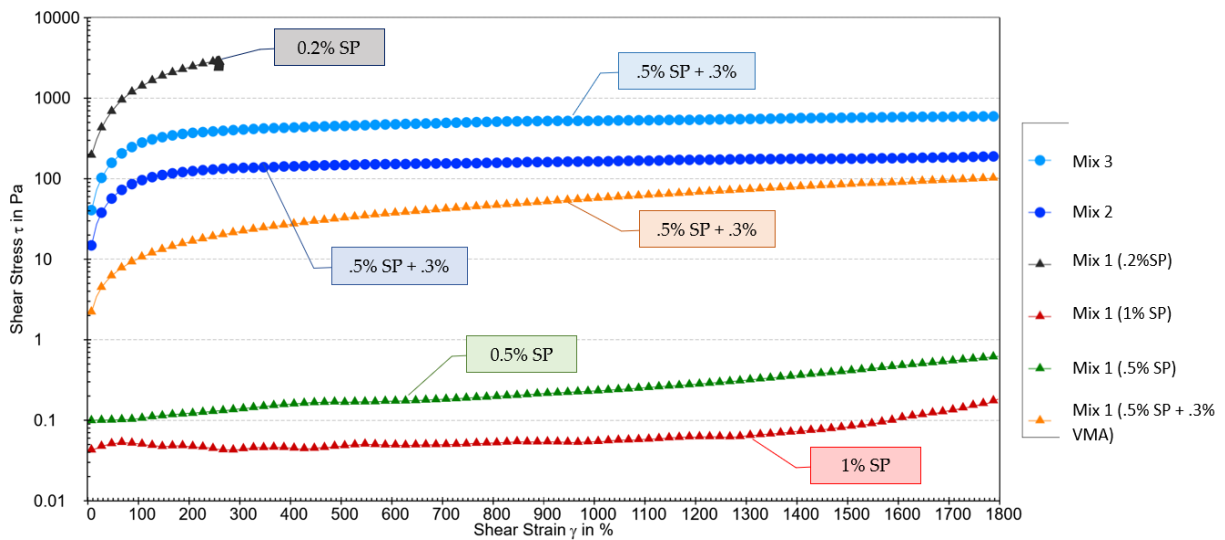


Figure 4: Shear stress strain graph showing all trials of the three different base mixtures investigated.

Initial Rheology Testing Matrix on Mix 1 and Mix 2

The development of a testing matrix to look at the static yield stress and identify any lingering problems regarding the testing was completed. Using the information gained from the initial rheology trials, a testing matrix was established. The base mix 2 and 3, in Table 2, were chosen to further study in a formal testing environment. Mix 2 will now be referred to as Mix 1 and Mix 3 will be referred to as Mix 2. The mixes in the matrix had .5 weight percent of the binder of superplasticizer (SP). For these tests, VMA was added in two ratios, .1% (VMA1) and .2% (VMA2) of the binder weight. ANC was added at a percentage of either .2% (ANC1) or .4% (ANC2). The test matrix for all mixes is shown in Table 3. As shown in the table, the properties of the VMA and ANC were studied without the effects of fibers before performing tests with 1 vol% and 2 vol% fibers incorporated into the mixture. All tests completed at this stage were constant strain rate tests with a rate of .1/s for 3 minutes.

Table 3: Test Matrix; The SP, VMA and ANC are reported as percentages of the binder by weight. The fiber is reported as a percentage of the total mixture, by volume. All other values are reported in ratios with respect to the total weight of binders (Cement, Cement Type III, Fly Ash and Silica Fume).

Mix ID	Silica Sand	Cement Type I/II	Cement Type III	Fly Ash	Silica Fume	Water	Superplasticizer (SP)	Viscosity modifying Agent (VMA)	Attapulginite Nanoclay (ANC)	Fiber (volume %)
M1 - B	.4	.4	.03	.42	.15	.28	.5%	0%	0%	0
M1 - VMA1	.4	.4	.03	.42	.15	.28	.5%	.1%	0%	0
M1 - VMA2	.4	.4	.03	.42	.15	.28	.5%	.2%	0%	0
M1 - ANC1	.4	.4	.03	.42	.15	.28	.5%	0%	.2%	0
M1 - ANC2	.4	.4	.03	.42	.15	.28	.5%	0%	.4%	0
M1 - VMA1 + ANC1	.4	.4	.03	.42	.15	.28	.5%	.1%	.2%	0
M1 - VMA1 + ANC1 - 1%PVA	.4	.4	.03	.42	.15	.28	.5%	.1%	.2%	1 vol%
M1 - VMA1 + ANC1 - 2%PVA	.4	.4	.03	.42	.15	.28	.5%	.1%	.2%	2 vol%
M2 - B	.4	.61	.07	.2	.13	.37	.5%	0%	0%	0
M2 - VMA1	.4	.61	.07	.2	.13	.37	.5%	.1%	0%	0
M2 - VMA2	.4	.61	.07	.2	.13	.37	.5%	.2%	0%	0

M2 - ANC1	.4	.61	.07	.2	.13	.37	.5%	0%	.2%	0
M2 - ANC2	.4	.61	.07	.2	.13	.37	.5%	0%	.4%	0
M2 - VMA1 + ANC1	.4	.61	.07	.2	.13	.37	.5%	.1%	.2%	0
M2 - VMA1 + ANC1 - 1%PVA	.4	.61	.07	.2	.13	.37	.5%	.1%	.2%	1 vol%
M2 - VMA1 + ANC1 - 2%PVA	.4	.61	.07	.2	.13	.37	.5%	.1%	.2%	2 vol%

A standard mixing procedure was developed to ensure a consistent time and order of mixing. Each type of admixtures used required a slightly different mixing procedure and can be summarized into four main mixing procedures: procedure for mixes with only VMA, procedure for mixes with only ANC, procedure for mixes with ANC and VMA and procedure for mixes with VMA, ANC and PVA fibers. These four procedures are shown in Fig. 5. The procedures all have 12 minutes of mixing time, with the exception of the VMA, ANC and PVA fibers procedure, which needed 3 additional minutes for fiber dispersion. Furthermore, the water was added in multiple steps during the procedure. This accomplished two things. First, suspending the admixtures (VMA, SP and ANC) in water before adding them, helps to ensure that none of measured liquids are stuck to the sides of the measurement beaker. Second, by adding VMA and ANC after the PVA fibers, the fibers are able to be incorporated into a mixture that has a low viscosity – this is expected to help achieve a uniform fiber dispersion.

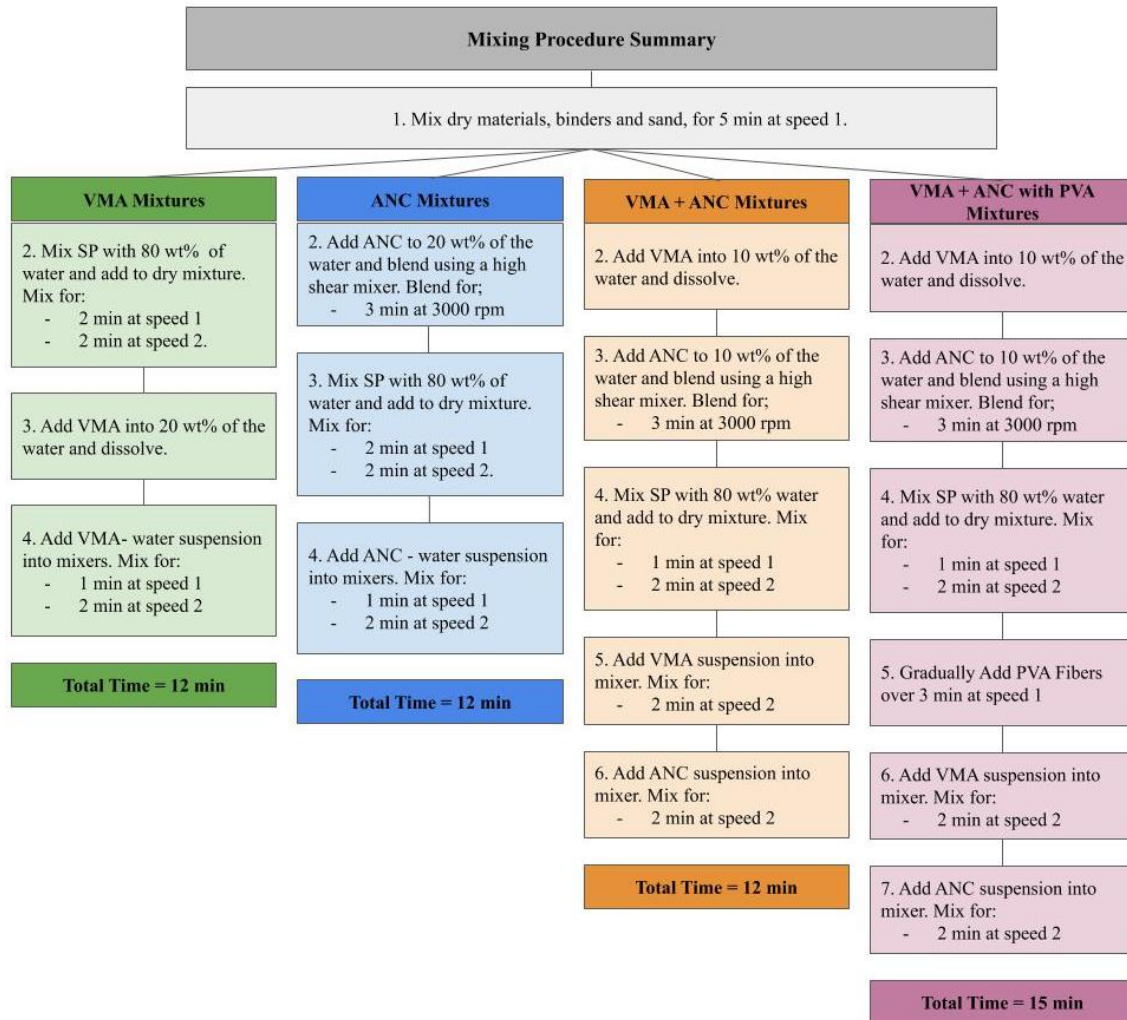


Figure 5: Summary of mixing procedure used in the testing matrix.

The testing matrix was completed using the mixing procedures shown in Fig. 5. and the results are shown in Fig. 6. It can be seen that the addition of VMA, ANC and fibers all raised the static yield stress of the mixture, as expected. Furthermore, it should be noted that several mixes reached the maximum limit of the rheometer and as a result an accurate yield stress could not be determined. For Mix 1, Fig. 6 (a), the mixture containing 2 vol% maxed out the rheometer after about 30 seconds. For Mix 2, the 2 vol% PVA fibers mix had too large of a shear stress to even begin a test. None of the mixtures that were able to be measured had a printable consistency.

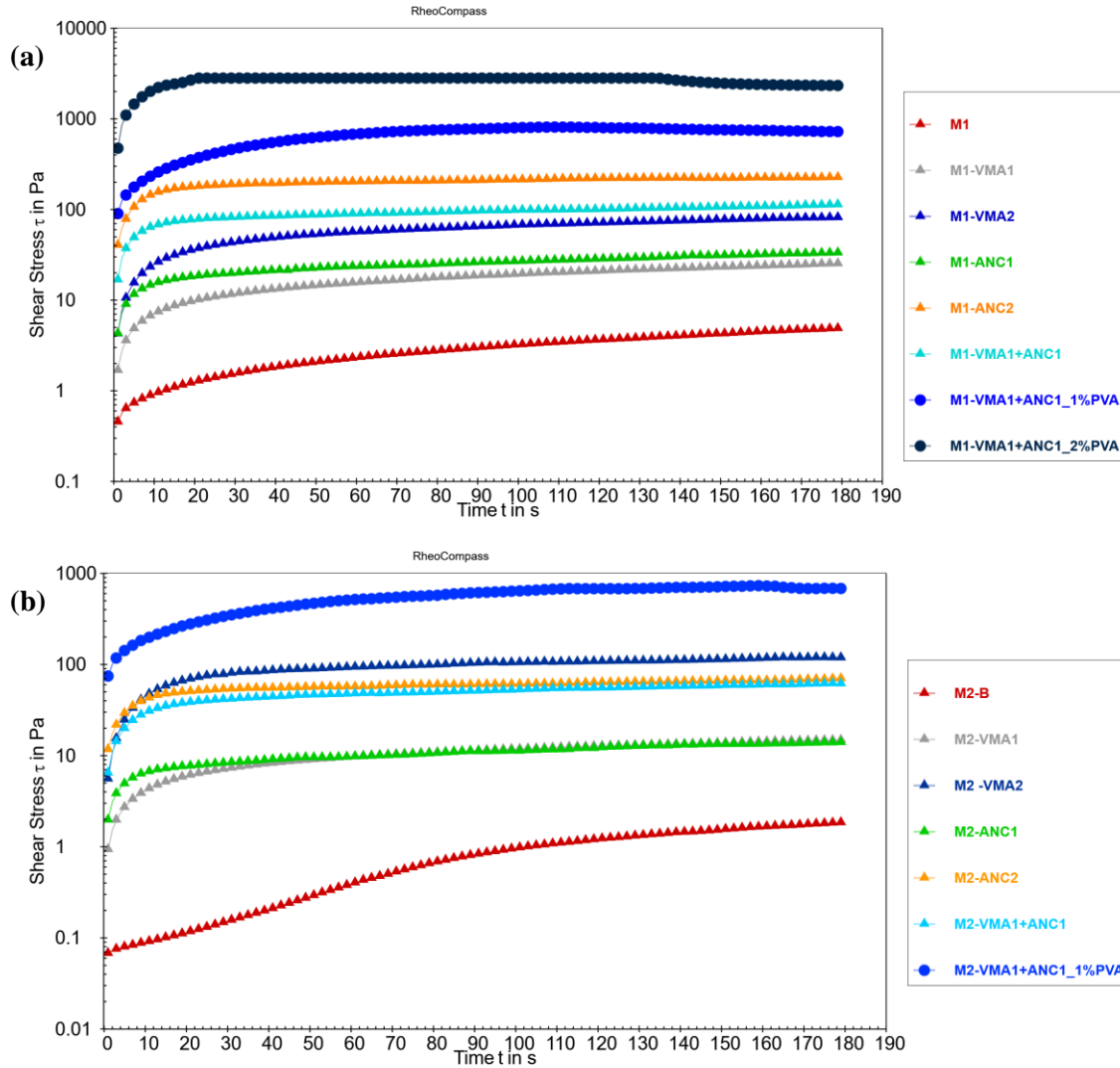


Figure 6: Evolution of shear stress vs. time of (a) Mix 1 and (b) Mix 2

While the results of the first testing matrices yielded encouraging and informative results, two challenges were encountered during the testing of the mixtures that included fibers. (1) The current shear vane used in the rheometer can read a maximum shear stress of 2814 Pascals, since the viscosity of fibrous mixtures is often higher than this, it is not possible to exactly measure a wide range of fiber reinforced mixtures. (2) The fibers in the mixtures had a tendency to clump together and leached water out at the edges - this was especially noticeable in the mixtures containing two volume percent of fibers, as shown in Fig. 7. These issues were addressed in the next round of testing. A new shear vane was purchased and used to measure much higher stresses than previously possible. To address the clumping of fibers, it was suggested that replacing the older cement type III cement with a fresh bag of calcium sulphoaluminate cement (CSA), a different type of quick setting cement, would help reduce the clumping.



Figure 7: Photos taken of the M1 - VMA1+ANC1 - 2%PVA (left) and M2 - VMA1+ANC1 - 2%PVA (right) highlighting the clumping of the fibers after mixing.

Rheology Testing Matrix and Admixture Optimization

Rheology Methods

In order to select a final mixture, the rheological properties of the mixes had to be further characterized beyond that of yield stresses and the issues identified in the preceding section had to be resolved. The admixtures needed to be optimized, in order to select the best possible mixture. This work was very extensive and required collaboration beyond that of just the Capstone team. Thus, this task was developed into a paper for the SPIE Smart Structures and Nondestructive evaluation 2021 conference proceedings (Schulte et al., 2021). This paper was worked on extensively by Ugur Kilic, a graduate student in Prof. Ozbulut’s research group, in conjunction with the Capstone Team. The results of this study are briefly summarized below and discussed in the context of this Capstone project.

The issues presented in the previous section were resolved by the purchasing of a new shear vane capable of measuring much higher yield stresses. Furthermore, in an attempt to fix the fiber clumping issue, the cement type III was replaced with CSA cement. Using insights from the previous section, base mix 2, based off of Soltan and Li, was selected for further analysis (Soltan & Li, 2018). The mixture design was first refined in order to more closely follow the original author’s design. The refined mixture is shown in Table 4. Additionally, this mixture contained an expansive agent (EA), an admixture intended to reduce shrinkage and drying related cracking. Furthermore, the trials were conducted with a constant amount of superplasticizer (SP) and variable amounts of VMA and ANC. The study was conducted with an analysis of variance (ANOVA) statistical method. Both VMA and ANC were studied in four different sublevels each. VMA was studied with 0%, 0.1%, 0.2% and 0.3% and ANC was studied in amounts of 0%, 0.2%, 0.4% and 0.6%. The factorial design is shown in Table 5. The static yield stress, dynamic yield stress, viscosity, thixotropy and structural recovery rate were examined as a function of VMA and ANC content. These properties were measured using stress growth tests, shear stress ramp-up tests and structural recovery tests, described in more detail in the next section.

Table 4: Material amount in revised Mix 2 given in ratio to total binder. Binders are taken to be Cement, CSA, Silica Fume and Fly Ash.

Portland Cement	CSA	Silica Fume	Fly Ash	EA	Sand	Water	SP
.682	.05	.05	.218	.03	.517	.37	.012

Table 5: Factorial Design of rheology tests

	ANC/b			
VMA/b	0%	0.2%	0.4%	0.6%
0%	Mix 1	Mix 2	Mix 3	Mix 4
0.1%	Mix 5	Mix 6	Mix 7	Mix 8
0.2%	Mix 9	Mix 10	Mix 11	Mix 12
0.3%	Mix 13	Mix 14	Mix 15	Mix 16

The materials were prepared using the same mixing procedure, as outlined in Fig. 5. The basic rheological properties of these mixtures were studied first without fibers and then promising mixtures were selected for study with fibers. An overview of the testing procedure used for each of the rheology tests is shown in Fig. 8. The stress growth protocol is a method in which a constant shear stress is applied to the mixture and the resulting stress is measured. The peak value of this stress is taken to be the static yield stress. The ramp test protocol has two main steps, the pre-shearing step and the data-logging step. The pre-shearing step is included in order to increase the homogeneity of the mixture and ensure a constant shear history between samples. The data obtained from this test can be fit using the Bingham model to calculate the dynamic yield stress and apparent viscosity. Both the stress growth protocol and ramp test protocol were performed on all of the mixes. The structural recovery tests were performed on select promising mixtures. The shear strain rates in this test were designed to mimic the deposition process, by mimicking the initial rest, extrusion and post-extrusion rest. The purpose of this test is to assess how much of the static yield stress of a certain mixture is recovered after extrusion. More detailed information can be found in the conference paper.

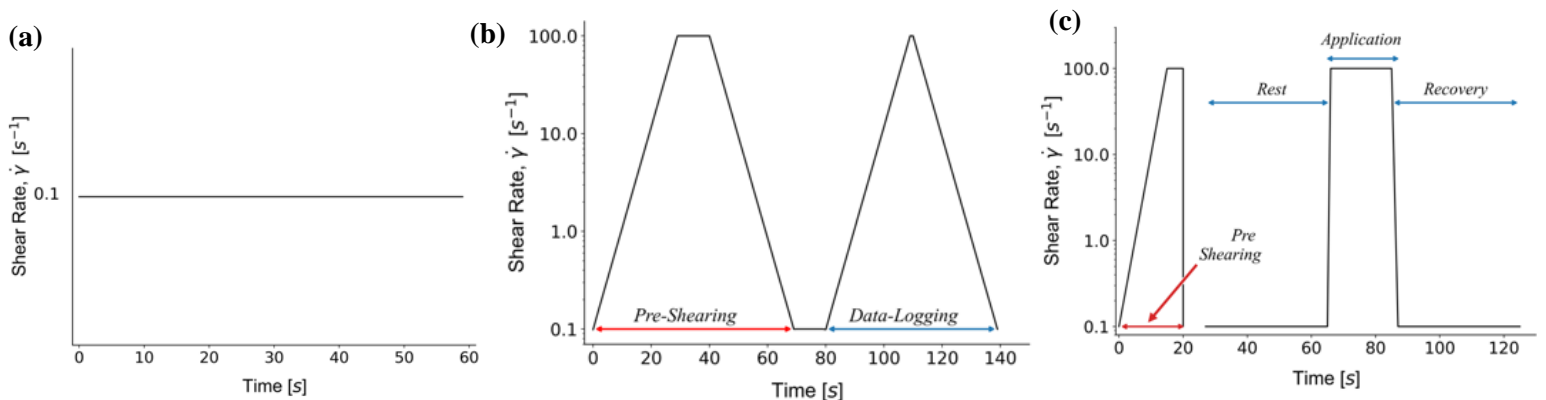


Figure 8: (a) stress growth protocol, (b) ramp test protocol and (c) structural recovery test protocol

Rheology Results and Discussion

The results of these trials are summarized below in Fig. 9 through Fig. 12. The static yield stress is defined as the stress required to initiate flow. This property is important when considering the buildability of the mixture, as the deposited layer will need to support the weight of subsequent layers. The plastic yield stress is the stress required to maintain flow. This property is important during the extrusion process, because it quantifies the stress needed to keep the material flowing through the nozzle. Furthermore, the apparent viscosity, AKA the resistance to flow, lends insights into the extrusion process as well. So does the thixotropy, which describes the decrease in viscosity when a shear stress is applied. A successful mixture will have a high static yield stress and thixotropy, while also having a low dynamic yield stress and viscosity. As it can be seen from the results in Fig. 9-12, none of the mixtures exhibit all of these traits. A high static yield stress and a low plastic viscosity were considered to be the salient conditions for producing a printable mixture, as they provide information about both the extrudability and buildability. Using this metric, Mix 8 and Mix 16 were selected as the most promising mixes, as they show the highest static yield stresses and lowest viscosities, while displaying acceptable values for the dynamic yield stress and thixotropy values.

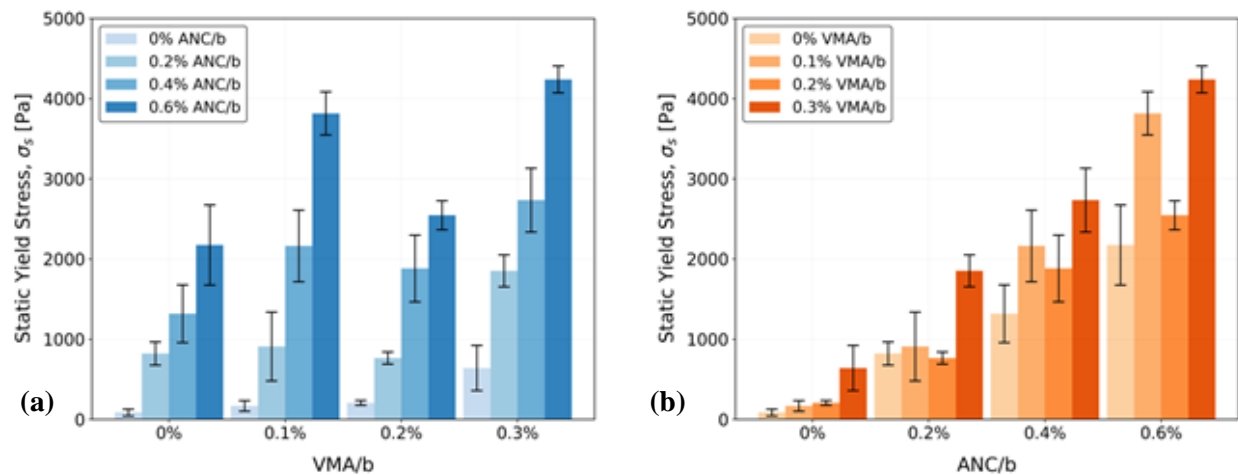


Figure 9: Effects of ANC and VMA on the static yield stress as a function of (a) VMA and (b) ANC.

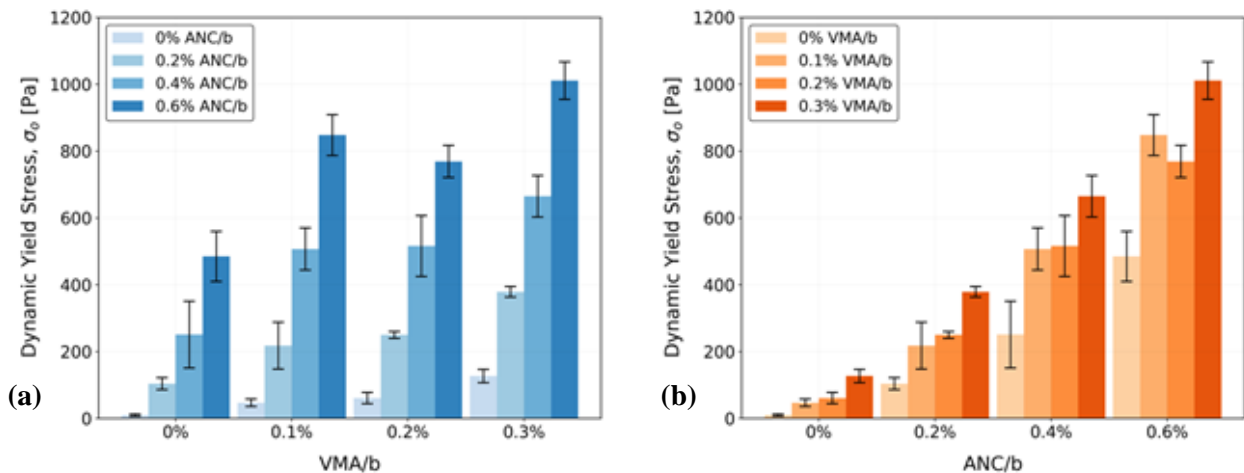


Figure 10: Effects of ANC and VMA on the dynamic yield stress as a function of (a) VMA and (b) ANC.

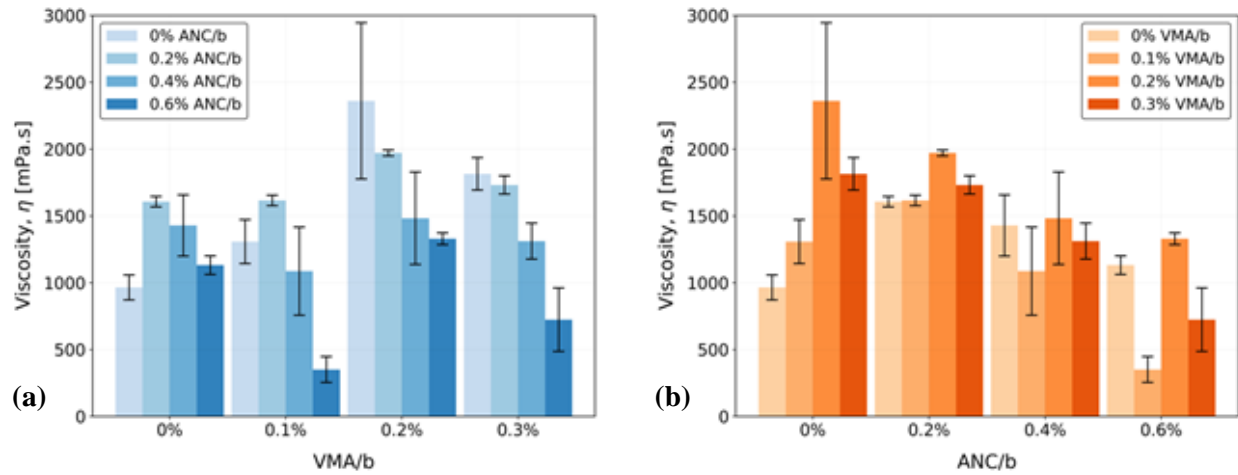


Figure 11: Effects of ANC and VMA on the viscosity as a function of (a) VMA and (b) ANC.

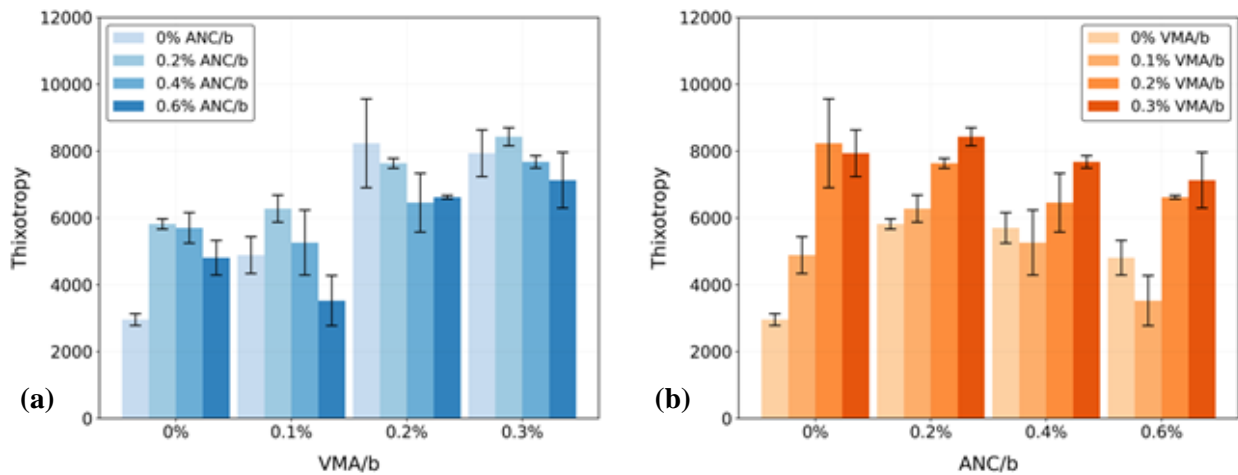


Figure 12: Effects of ANC and VMA on the thixotropy as a function of (a) VMA and (b) ANC.

In the conference paper, these mixtures were studied with fiber percentages of 0%, 0.25%, 0.5% and 1% by volume. Mix 8 and Mix 16 were selected to do a structural recovery test shown in Fig. 13. Based on these results, it can be seen that Mix 8 with 0.5% fibers displayed the fastest structural recovery rate, reaching over 80% of the initial viscosity in just under 10 seconds. Based on these results, a buildability study was conducted on Mix 8 with 0.5% PVA fibers. The buildability trial was very successful, as it produced a 32-layer high wall before it collapsed due to elastic buckling.

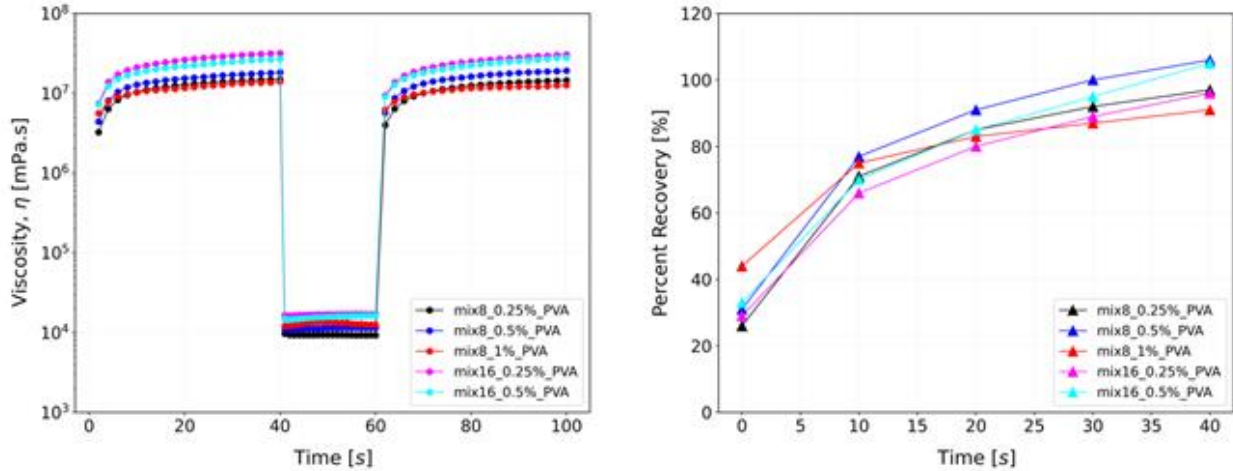


Figure 13: The results of the structural recovery testing of Mix 8 and Mix 16 with fiber percentages of 0%, 0.25%, 0.5% and 1%.

The results obtained in the related study for the SPIE conference paper were leveraged to decide which mixture was used to print the optimized beam. Based on the results, Mix 4 and Mix 8 were used to fabricate the mechanical specimens. Mix 8 was shown previously to be printable in conference paper with .5% PVA, therefore it was selected for further study based on prior success. Since fibers had been shown to increase the yield stress in the conference paper, it was unclear whether Mix 8 with its high yield stress and low viscosity, will still be extrudable with a higher fiber amount. With this in mind, Mix 4 was also selected for study, as it has a moderate yield stress and moderate viscosity, so it may be able to better handle the increase in yield stress associated with fibers.

Mechanical Testing

Specimen Creation and Test Matrix

The next stage of the project is the flexural testing of the mixtures. This section was designed to answer several different questions; whether fibers are a valid form of reinforcement, whether the difference in admixtures between Mix 4 and Mix 8 or a change in tool path (the path that the nozzle takes to lie down the layers) results in different mechanical properties. And finally, to see how an AM fabricated sample compares to a traditionally cast sample in terms of strength. In order to achieve this, the fiber reinforced samples will contain 1 vol% of fibers. Other researchers have suggested that fiber amounts in excess of 1 vol% is necessary to replace steel reinforcements (Hambach & Volkmer, 2017), with many studies examining mixtures containing 2 vol% of fibers (Figueiredo et al., 2019; Soltan & Li, 2018; Zhu et al., 2019). However, 1 vol% was selected, as it was discovered that the fibers clogged our 10 mm nozzle at higher fiber percentages. This issue was only amplified as the fiber clumping, as shown in Fig. 7, was still present. The replacement of Cement Type III with CSA cement helped, but did not completely resolve the issue. This change to 1 vol% fibers was not viewed as detrimental to our project goals, as the main purpose of this study will be to compare the properties of AM versus cast in place, as well as the effects of tool paths. This study will expand the capabilities of the lab to study fiber reinforced concrete and future projects may study mechanical properties with higher fiber percentages.

The mechanical test specimens were selected to be 3''x1.5''x12'' (width, height, length) and fabricated with two different tool paths on the AM printer and using concrete molds. Creating the tool paths for the AM samples with GCode was proved to be complicated, as the printer had a customized software that wasn't compatible with software generated GCode. Rather than taking code generated by existing software and modifying it to conform with the nuances of the custom printer, the code was instead generated using excel spreadsheets, as shown in Fig. 14. With some troubleshooting, this code proved to work with the printer and was used to print the mechanical testing specimens.

Sample	Layer	G28	X	Y	Z	E	F	Initial X	Initial Y	Initial Z	Initial E	Initial F	nozzle	layer height	Specimen length	Specimen width	Specimen height	Path 1 X length	Path 1 Y length	Path 2 X length	Path 2 Y length	E	F	Up at layer end	Distance between sat
1	1	G1	X	600	Y	0	Z	235	E	0	F	1000	G1 X600 Y0 Z235 E0 F1000												
1	1	G1	X	676	Y	0	Z	235	E	76	F	5000	G1 X676 Y0 Z235 E76 F5000												
1	1	G1	X	600	Y	10	Z	235	E	86	F	5000	G1 X600 Y10 Z235 E86 F5000												
1	1	G1	X	600	Y	10	Z	235	E	162	F	5000	G1 X600 Y10 Z235 E162 F5000												
1	1	G1	X	600	Y	20	Z	235	E	172	F	5000	G1 X600 Y20 Z235 E172 F5000												
1	1	G1	X	676	Y	20	Z	235	E	248	F	5000	G1 X676 Y20 Z235 E248 F5000												
1	1	G1	X	676	Y	30	Z	235	E	258	F	5000	G1 X676 Y30 Z235 E258 F5000												
1	1	G1	X	600	Y	30	Z	235	E	334	F	5000	G1 X600 Y30 Z235 E334 F5000												
1	1	G1	X	600	Y	40	Z	235	E	344	F	5000	G1 X600 Y40 Z235 E344 F5000												
1	1	G1	X	676	Y	40	Z	235	E	420	F	5000	G1 X676 Y40 Z235 E420 F5000												
1	1	G1	X	676	Y	50	Z	235	E	430	F	5000	G1 X676 Y50 Z235 E430 F5000												
1	1	G1	X	600	Y	50	Z	235	E	506	F	5000	G1 X600 Y50 Z235 E506 F5000												
1	1	G1	X	600	Y	60	Z	235	E	516	F	5000	G1 X600 Y60 Z235 E516 F5000												

Figure 14: Sample of manually written GCode for Beam Tool Path 1

The challenges associated with the GCode generation are one reason the original scope of designing a unique beam geometry was changed. Rather than a more optimal beam design as the stress analysis studies (shown in later sections) had intended, tool path was instead compared between the additively manufactured beams. The differing tool paths are shown in Fig. 15. The Tool Path 1 deposited concrete in lines parallel to the long side of the beam, while Tool Path 2 deposited lines parallel with the short side of the beam. Both GCodes were coded to deposit the correct number of lines and layers to manufacture specimens to be a final dimension of 3 x 1.5 x 12 inches (height x width x length). Other toolpaths were proposed such as a diagonal one, much like what consumer 3D printers use. However, these proved too difficult to manually code, and these two were used instead. Comparison of these two is expected to show significantly different strengths given the stress concentrations of the printed geometry and the orientation of bonded layers relative to applied load. For the traditionally cast beams, the capstone team fabricated our own molds using the design in Fig. 16, which is intended to produce twelve 3''x1.5''x12'' beams concurrently.

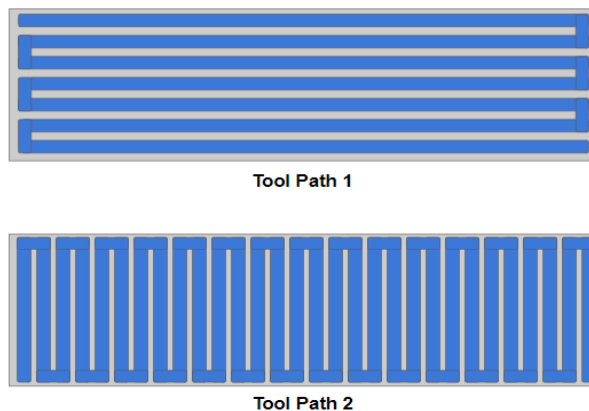


Figure 15: Different Toolpaths that the AM specimens will be fabricated using.

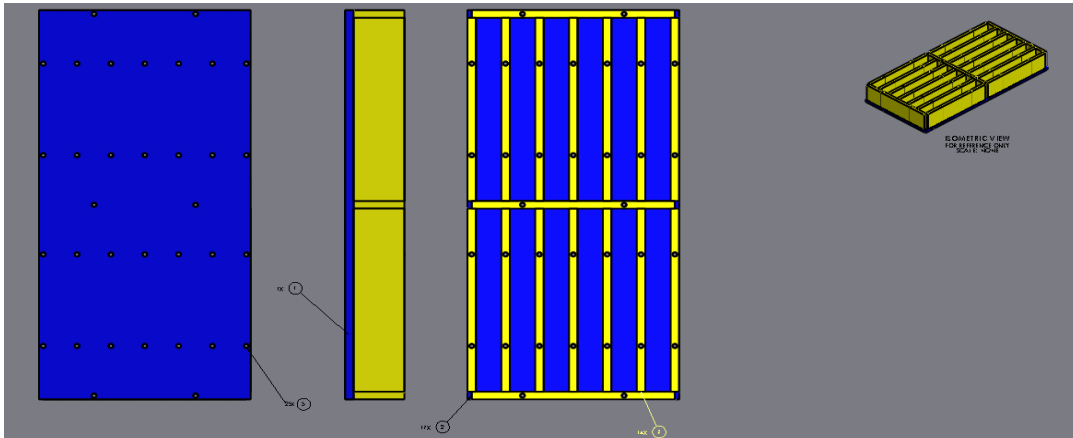


Figure 16: Final concrete Mold Design

The final testing matrix for the flexural testing includes the AM fabrication of beams with Mix 4 and Mix 8 with 1 vol% of PVA fibers printed in tool path 1 and tool path 2, Table 6. Furthermore, samples will be cast with both Mix 4 and Mix 8 with both 0 vol% fibers and 1 vol% fibers. Three specimens of each type were fabricated and tested to ensure repeatable results. The testing matrix is summarized in table #, with the shorthand ID's summarized. Furthermore, the first specimen for the cast mix 8 with 1 vol% PVA (M8-1F-1) fiber was damaged prior to testing, and as such was excluded from the analysis. However, the remaining two specimens had tight agreement in mechanical properties, so the properties are believed to be accurately represented.

Table 6: Mechanical Testing Matrix for Flexural Testing

	Cast				AM			
	0% PVA Fibers		1% PVA Fibers		1% PVA w/ Tool Path 1		1% PVA w/ Tool Path 2	
	Mix 4	Mix 8	Mix 4	Mix 8	Mix 4	Mix 8	Mix 4	Mix 8
Replicate 1	M4-0F-1	M8-0F-1	M4-1F-1	M8-1F-1	M4-TP1-1	M8-TP1-1	M4-TP2-1	M8-TP2-1
Replicate 2	M4-0F-2	M8-0F-2	M4-1F-2	M8-1F-2	M4-TP1-2	M8-TP1-2	M4-TP2-2	M8-TP2-2
Replicate 3	M4-0F-3	M8-0F-3	M4-1F-3	M8-1F-3	M4-TP1-3	M8-TP1-3	M4-TP2-3	M8-TP2-3

The AM samples were printed with a 10mm diameter nozzle. Before printing the extrusion rate, printing speed, and force were altered to find the optimal combination for continuous printing. Furthermore, the samples were watched to ensure that the printed lines were continuous with minimal breaking. Pictures of all the specimens are shown in Fig. 17. Both the cast and AM printed specimens were cured in lab air for 28 days before testing, in order to replicate the field curing conditions.

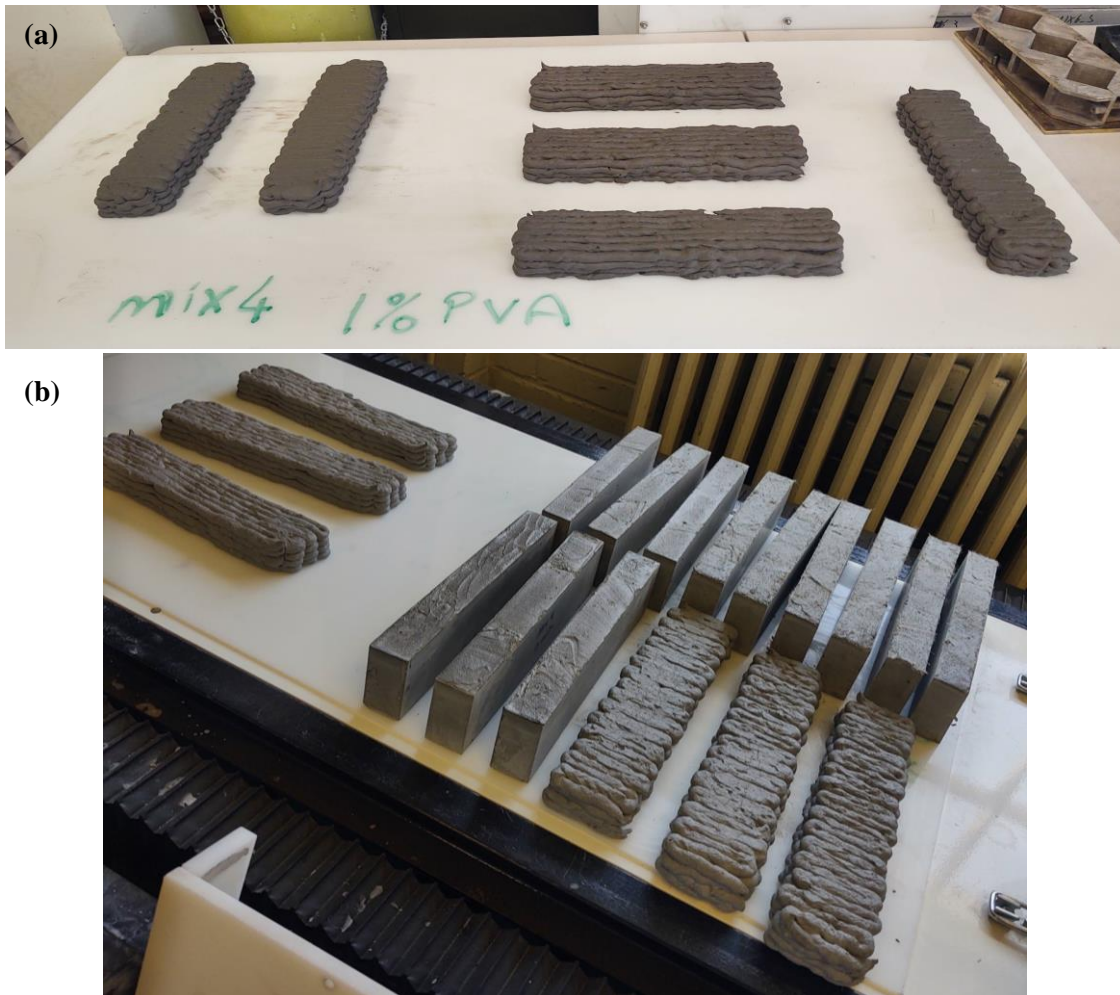


Figure 17: All mechanical specimens (a) Mix 4 showing both tool paths and (b) Mix 8 with both tool paths and all cast specimens

Testing Methods

A three-point bending (center point loading) flexural bending procedure was used to evaluate the mechanical properties. The samples were tested on an MTS 810 servohydraulic load frame equipped with a 22 kip load cell. The testing samples were oriented, so that the tests were weak axis bending with 3'' and 1.5'' being the width and depth, respectively. The span length of the specimens was 9''. This span was selected to be as close to conforming to standard practices as possible, while still being reasonable for our test setup. The loading rate was 75 lbs/min, which was calculated in accordance with ASTM C293, the testing set up is shown in Fig.18.



Figure 18: 3 Point Bending Flexural Testing Setup

After testing the beams, the loads and displacements were converted to flexural stresses and strains for all specimens, using the general flexural equations below:

$$\sigma_f = \frac{3FL}{2bd^2} \quad (1)$$

$$\epsilon_f = \frac{6Dd}{L^2} \quad (2)$$

Where, σ_f and ϵ_f are flexural stress and flexural strain, respectively. F and D are the load and deflection at a given time. L is the span length (9''), b is the width of the beam (3'') and d is the depth of the beam (1.5'').

Mechanical Testing Results

The flexural stress vs. strain curves of all the samples are shown in Fig. 19. It can be seen that all the mixtures containing fibers displayed a more ductile nature than the cast specimens with no reinforcement. Furthermore, the stress strain curves of all the fiber reinforced composites show strain hardening, with the exception of specimens printed in Tool Path 2. The maximum loads experienced by each specimen were used to calculate the flexural strengths, which are shown in Table 7 and Fig. 20.

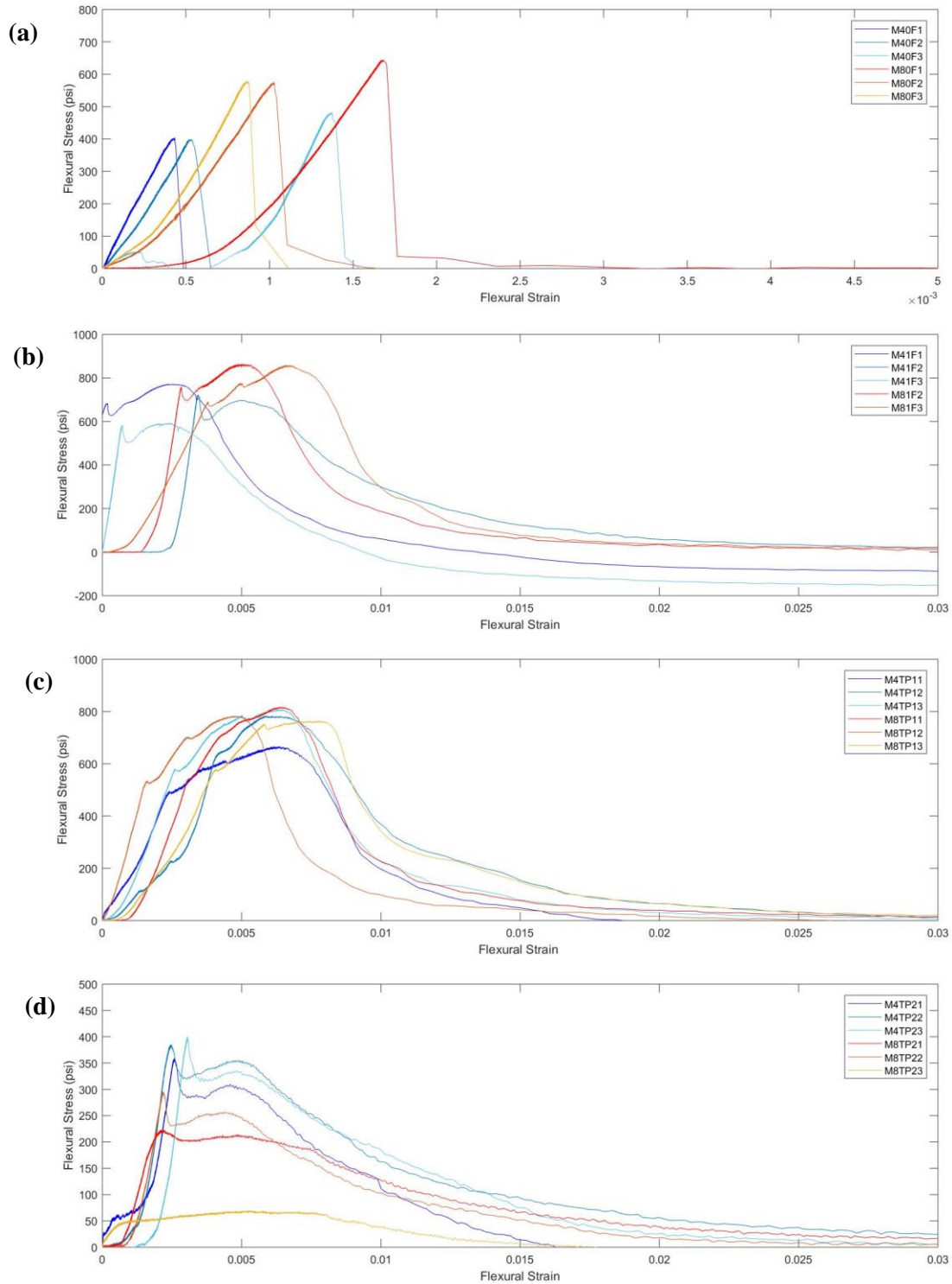


Figure 19: Flexural Stress vs. Strain Curves for the 3-point bending flexural testing, (a) Cast specimens with no PVA fibers, (b) cast specimens with 1 vol% PVA fibers, (c) AM printed samples in Tool Path 1 and (d) AM printed samples in Tool Path 2.

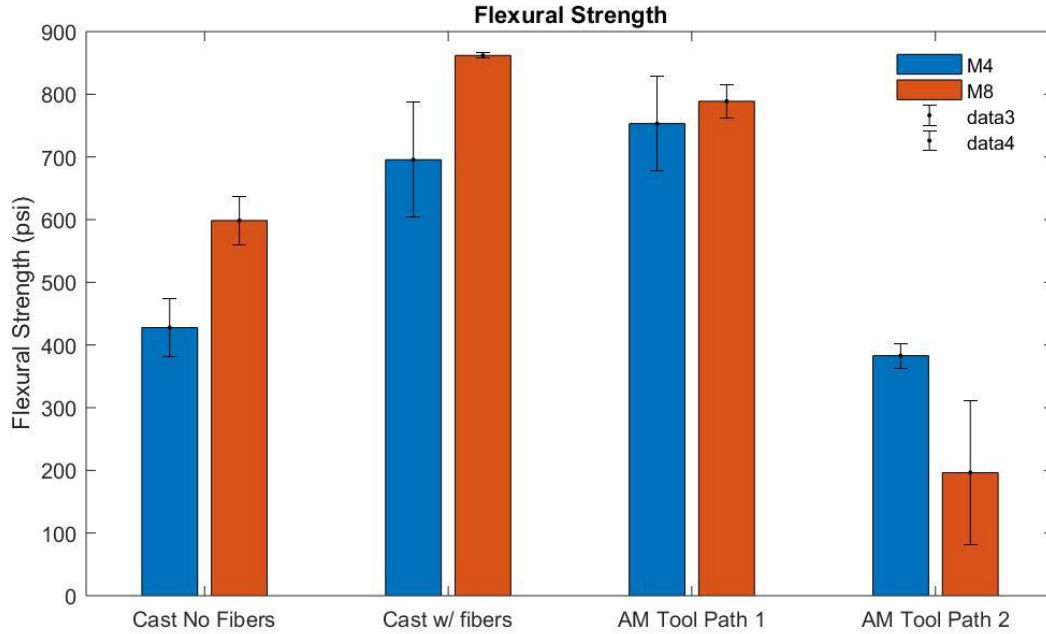


Figure 20: Bar graph comparing flexural strength of the samples with standard deviations.

Table 7: Average Flexural Strength of each Specimen type. Standard Deviations are shown in parenthesis.

	Cast No Fibers	Cast w/ Fibers	AM Tool Path 1	AM Tool Path 2
M4	427.7 (46.3)	695.6 (92.0)	753.2 (74.3)	382.8 (19.6)
M8	598.6 (39.1)	861.8 (4.0)	788.8 (27.0)	196.3 (115.1)

Furthermore, optical microscopy was done to assess the microstructure of the AM specimens. Special attention was paid to the fiber alignment within the printed layers. Other researchers have shown that for fibers longer than the nozzle diameter, there will be a preferential alignment along the printing direction (Hambach & Volkmer, 2017). However, the PVA fibers used in this study were shorter than the diameter of the nozzle (8mm vs. 10mm, respectively), thus it was necessary to determine any alignment was present. For the purposes of this study, the print direction in which the nozzle is moving and laying down material will be called the longitudinal direction (L), the upwards direction that the layers are being built up in is the short transverse direction (S) and the tertiary direction will be referred to as the long transverse direction (T). A Mix 4 Tool Path 1 sample was cut via a water jet and polished using Si-C polishing pads to a surface finish of 600 grit. The S-L and S - T were imaged in a Hirox Optical Microscope, in order to determine the fiber alignment in the AM printed specimens. Representative 50x images are shown in Fig 21. While a length view of a few fibers can be seen in the S-T face, primarily the 38-micron circular cross sections of the fibers are visible (denoted by the yellow arrows in Fig. 21). Conversely, in the S-L image, a much larger number of length-oriented fibers can be seen. These images suggest a preferential alignment of the fibers along the longitudinal direction.

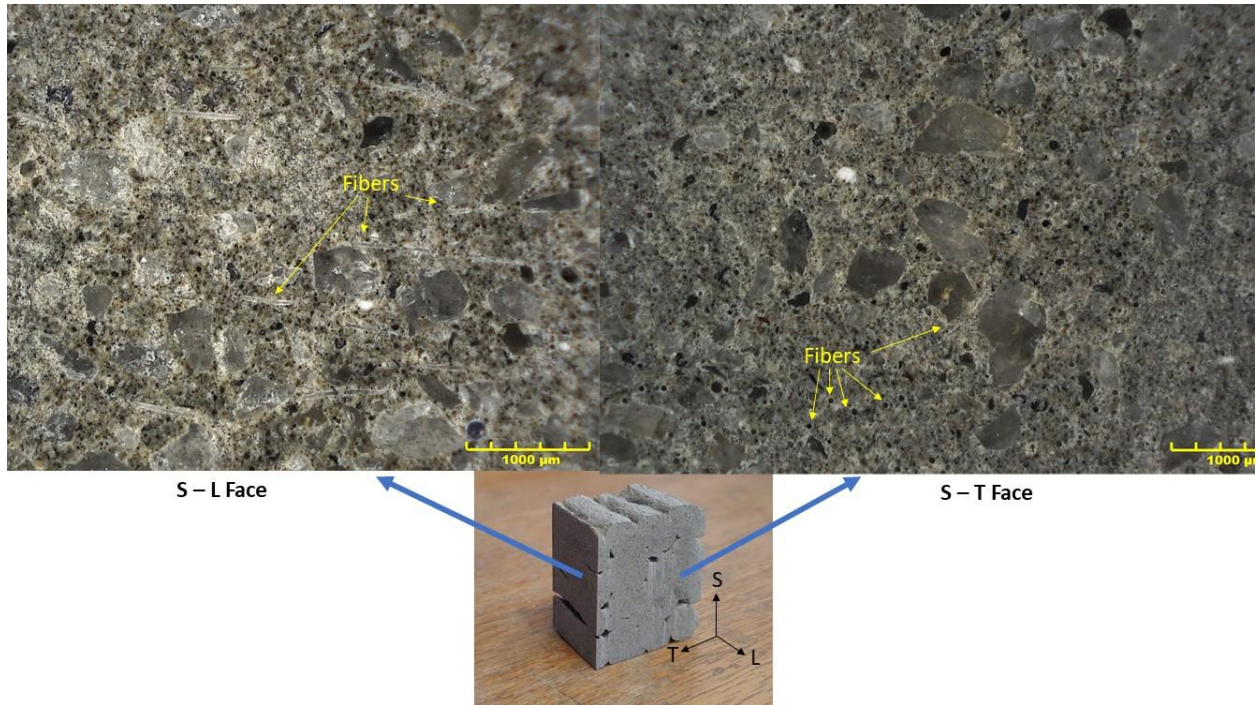


Figure 21: Schematic showing the microstructure of a Mix 4 Tool Path 1 beam, showing the figure alignment along the short transverse and longitudinal plane (S-L) and short transverse and long transverse plane (S - T).

Mechanical Testing Discussion

One question addressed by the mechanical testing, is whether the differing rheological properties of Mix 4 and Mix 8 had an effect on the final mechanical properties of the specimens. It appears that the cast specimens of Mix 8 had a higher strength than Mix 4. The two mixes had nominally the same strength in AM Tool Path 1 specimens and Mix 8 had a lower strength than Mix 4 for AM tool path 2. Furthermore, by comparing cast specimens with 0% PVA fibers and 1% PVA fibers, it is confirmed that fibers are a valid form of reinforcement, as the fiber containing specimens were significantly stronger. Both mixes had an increase in flexural strength of about 260 psi. This paired with the strain hardening characteristics displayed by the specimens containing fibers, proves the validity of self-reinforcement for this particular material. Soltan and Li, also, observed this strain hardening effect during their tensile testing of the mixture that inspired this one (Soltan & Li, 2018). However, while Tool Path 2 did show ductile behavior, it was the only fiber containing fabrication condition that did not show strain hardening behavior.

When comparing processing parameters, it is clear that Tool Path 1 has a higher flexural strength than Tool Path 2. This likely results from two main factors. When Tool Path 2 is tested the tensile forces in the bottom fibers of the beam are pulling along the transverse direction of the pieces. Thus, the boundaries between layers are aligned with the plane along which the failure occurs, providing a geometric stress concentration and making failure more dependent on adhesion between layers than overall matrix strength. Additionally, with the preferential alignment of the fibers along the longitudinal direction (print direction), the majority of fibers are not oriented correctly to carry tensile loads in Tool Path 2, but they are in Tool Path 1. Thus, the fibers are more effective as reinforcement in Tool Path 1.

Lastly, the AM specimens printed in Tool Path 1 had a comparable flexural strength to the cast specimens with 1 vol% PVA fiber. This confirms that the AM process in this study did not have a negative effect on the flexural strength. This result was likely due to two competing factors, the poor interlayer bonding and the fiber alignment in the AM samples. After failure, the cross sections of the AM samples were examined. It was clear that the layers were not completely bonded together, as there were noticeable gaps. A bar graph showing the max loads measured for Mix 8 Tool Path 1 samples and their corresponding cross sections are shown in Fig. 22. It can be seen from the figure that the cross sections with more visible interlayer gaps had a lower maximum load. This suggests that the gaps are serving as stress concentrators and have an effect on the overall strength. Furthermore, these images highlight the inconsistencies within AM samples printed with the same mixture and batch. The cross section for a representative cast specimen is shown in Fig. 22. The cast specimens had a much more uniform cross-sectional area, which would suggest a larger strength. However, the fiber alignment along the tensile loading direction in the AM Tool Path 1 specimens, serves to increase the strength. As the extrusion process is what aligns the fiber, there is no reason to suspect that the fibers will be aligned in the cast specimen. Other researchers have confirmed this (Zhu et al., 2019). From this data set, it appears that the effects of the stress concentrators in the cross section and the aligned fibers mostly cancel each other out and result in a similar flexural strength.

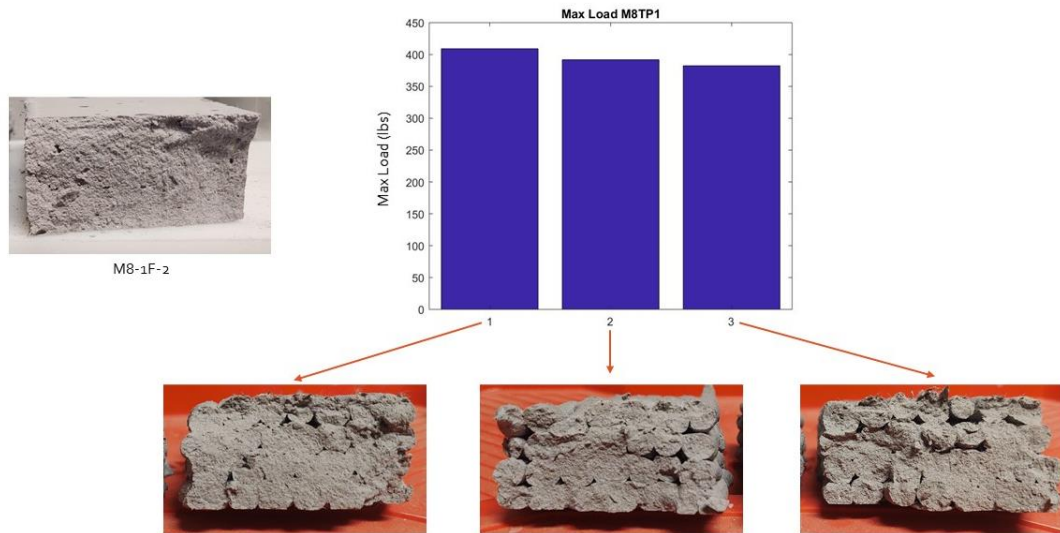


Figure 22: Comparison of AM specimen cross sections of Mix 8 Tool Path 1 with reference to the max loads. Cast Mix 8 with 1 vol% PVA fibers were added for reference

Modeling of Elastic Modulus

While the experimental data shows quantitatively which mixtures and manufacturing methods perform best, such data cannot be directly applied to future design efforts to build a structure. First, while factors like flexural strength are useful for comparison, material properties such as the Elastic modulus are required in order for informed design to occur. As a result, an attempt was made to replicate the results of the flexural testing with Solidworks Finite Element Analysis. In order to provide the most accurate replication, the refined mesh, shown in Fig. 23. was used instead of the coarse mesh used the geometric

optimization section. This made the results more valid, but in other sections would have significantly increased computation time.

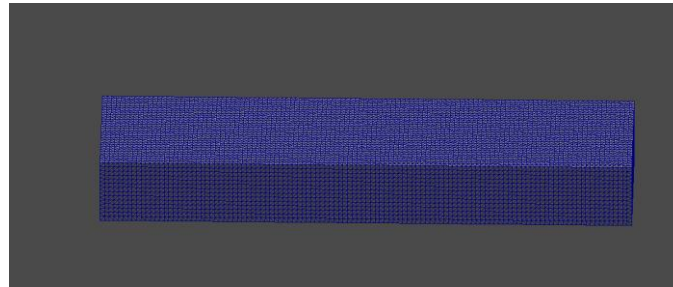


Figure 23: Fine Mesh used in Analysis

To start, material properties from Li were used (Li, 2008). Many of the properties shown in Fig. 24 are not directly relevant to stress analysis, but are asked for by the software. For the purposes of this analysis, density and elastic modulus are of most relevance, while values such as tensile and compressive strength can be checked manually against stresses that produce failure. Shear modulus and Poisson’s ratio would be useful in future developments, but should be tested more directly. For purposes of this analysis, values from the literature were used, with the elastic modulus being manipulated to conform with test data and produce failure.

Property	Value	Units
Elastic Modulus	4778993.456	psi
Poisson's Ratio	0.2	N/A
Shear Modulus	3045792.491	psi
Mass Density	0.03974001	lb/in ³
Tensile Strength	677.3262349	psi
Compressive Strength	7204.02443	psi
Yield Strength	435.113213	psi
Thermal Expansion Coefficient	55555.55556	/°F
Thermal Conductivity	6.68738e-06	Btu/(in·sec·°F)
Specific Heat	0.179134	Btu/(lb·°F)
Material Damping Ratio	0.05	N/A

Figure 24: Starting Properties of ECC, which were adjusted to conform with test data

Analysis was done by taking the maximum load produced by the two highest strength samples, Mixture 8’s cast and printed example, and applying it in the same 3 PT bending setup as the test samples were subjected to. This is shown in Fig. 25 (a), where the beam has been sectioned to display the stresses along the midplane of its cross section, where load is applied. Visual distribution of these stresses are shown in Fig, 25 (b), where it can be seen that stresses are primarily in the tension and compression faces, and are similar in magnitude.



Figure 25: A) FEA Setup for Analysis, with Stress Plot B) Visual Stress distribution along Analyzed Beam Cross Section

Plotting the stress along the centerline of this face produces the plot in Fig. 26, where the flexural strength was reached at the compression face. While this plot displays stresses as all positive, in fact the stresses on the left side of the plot (top of the cross section) are compressive and those below the minimum, in tension. Based on the location of this minimum, it can be seen that the neutral axis appears slightly below the centerline, which had been manipulated in prior analysis runs for optimization. Seeing this stress distribution of the tested beam gives some indication to the kinds of area reductions that could be done in future studies to achieve a similar strength with reduced mass.

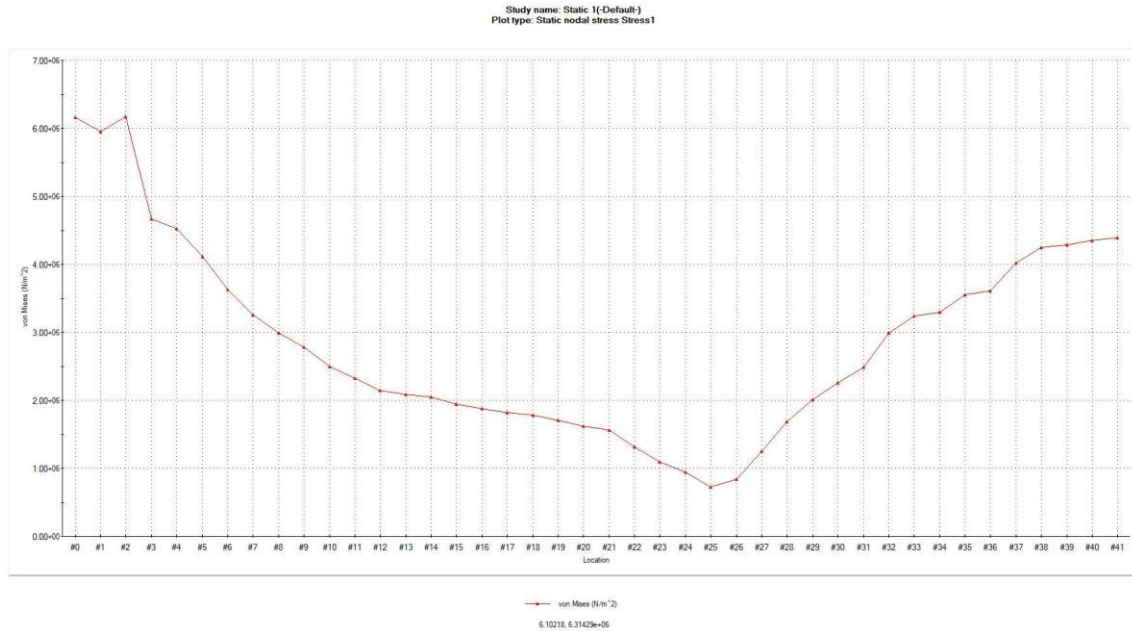


Figure 26: Graphical Stress Distribution along analyzed beam cross section

Through manipulation of elastic modulus at given peak loads and flexural strength of the mix 8 beams shown in Table 8, it can be seen that there is an appreciable difference in elastic modulus based on the additive manufacturing process. 2 factors likely affect this, one being artificial. By virtue of the nozzle size and size of fibers, fibers in the toolpath 2 example can be aligned with the tensile direction of the beam face, enhancing the tensile properties compared to the cast example. This is counteracted by large voids in the cross section that reduce the area over which stresses are distributed. For more robust results, further testing will be needed that includes other aspects of the material than flexural strength, such as direct tension or compression tests. But these results indicate that Mix 8 is the most likely candidate for further development, and that its additively manufactured state might even improve its performance.

Table 8: Results of FEA of Printed Beam

	M8, Cast	M8, Toolpath 1
Applied Peak Load (lbs)	400	380

Flexural Strength (PSI w/ STD Dev)	861.8 (4.0)	788.8 (27.0)
Expected Elastic Modulus (psi)	4.68×10^6	3.7×10^6

Geometry Optimization

The geometric optimization and stress analysis that was performed before the scope of the study shifted to include tool paths is included in this section. Even though an optimized beam was never printed in this capstone, these studies still provide valuable information for future studies.

Understand tensile stresses in small scale beams

Using a study of small scale fiber reinforced beams by Yu et al. from Tonji University, peak loads on the small scale beams from their study were applied to models in 2 separate systems (Yu et al., 2018). First, a standard set of shear force and bending moment diagrams were generated in SkyCiv, a matrix method based structural design software similar to SAP2000. This generated the standard set of data one might calculate by hand. In addition, the finite element model, shown below in Fig. 27, was created in Solidworks to better understand the exact distribution of stresses in the beam. However, direct comparison with data in this study proved difficult, so another approach was taken to give a general idea of the capacity of a small-scale beam like this. This could have been the result of a calculation error on either side, as attempts to manually calculate observed values with the given material data were roughly 1 order of magnitude different than observed. In the end, this manual calculation was supplemented with computer modeling to eliminate much of the potential for numerical errors.

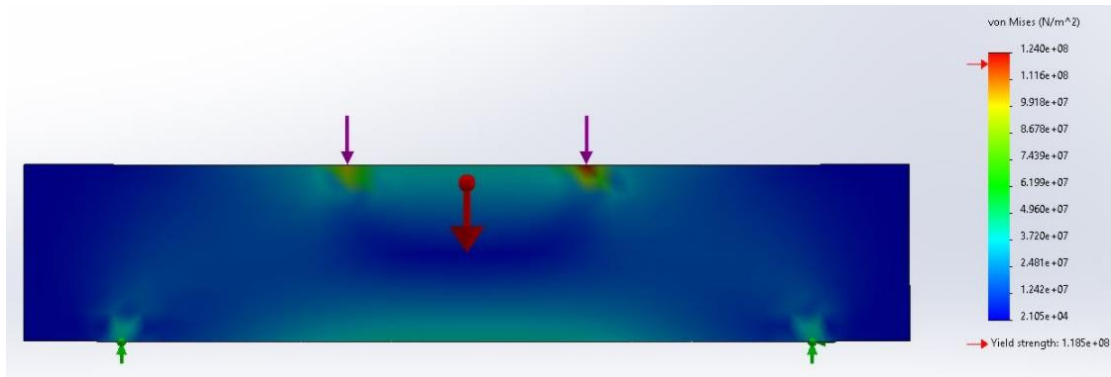


Figure 27: Finite Element Model of 4 Pt Bending in small Scale Concrete Beam

To resolve this issue, a MathCAD sheet was used to determine moment capacity of reinforced beams used in the study. This presented some difficulty, as units in the study were metric and ACI codes generally operate in imperial. Through some iterations, a moment capacity similar to that displayed by the beams in the study was found, validating the modeling method for use in later studies.

Early Optimization of Beam Member

Using the rough scale of the beams tested in the above study (100x100x500mm), and the same 4 pt. bending test, several iterations of different geometries were performed to understand how best to reduce tensile loads and relieve weight in these beam cross sections. This began with the simple use of an I style cross section as opposed to the standard square, Fig. 28 bottom image. Weight relieving slots were gradually added to lower stress regions.

Following this, a study by Audibert, et al. was used to more scientifically approach the topic of weight relief (Audibert et al., 2018.). These beams follow a bio-inspired approach replicating bone structures of mammals and birds to better distribute stresses. These were optimized for 3 pt. bending tests, which were ultimately performed in the lab. However, at the time 4 pt bending seemed more logical as other studies used it in their modeling. Results of the tests are similar in either case, so analysis was not redone with 3 pt bending. Currently, these methods seem promising, but printability with concrete of a given layer height must still be verified.

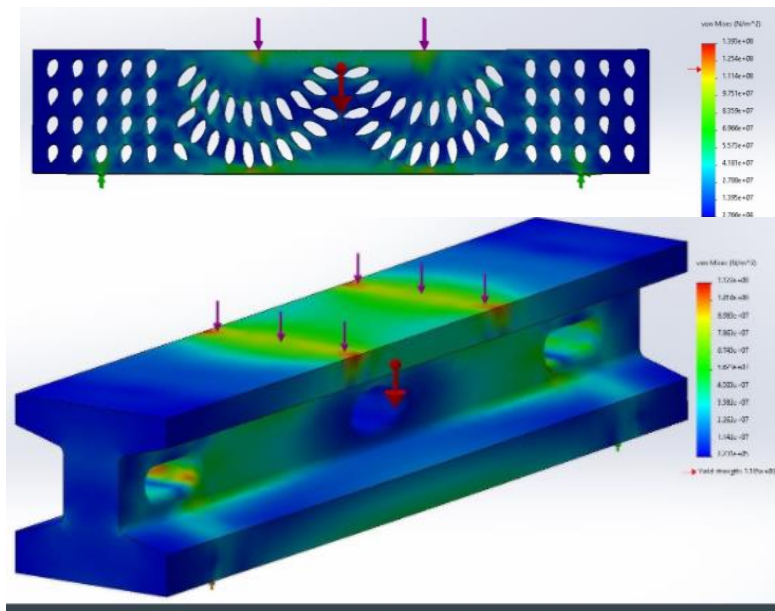


Fig. 28: Finite Element Models of Early Optimized Geometry Beams

Stress Block Analysis of ECC

To use a more standardized method of analyzing these concrete beams, MathCAD sheets and excel documents were used to explore the moment capacity of unreinforced concrete beams. These efforts were utilized in order to understand what material and geometric factors could be altered to produce the greatest likelihood of a successful final beam. The MathCAD sheet shown in Fig. 29 calculates capacities for unreinforced rectangular sections, and is provisioned to allow both tension and compression-controlled cases. However, its usefulness is limited to rectangular sections, as the equations for even simple alternatives such as trapezoids require integration. In conjunction with excel, however, this can lend insight into which material properties should be targeted to increase capacity. This lends understanding about

whether strain capacity or pure tensile strength is of more concern in design.

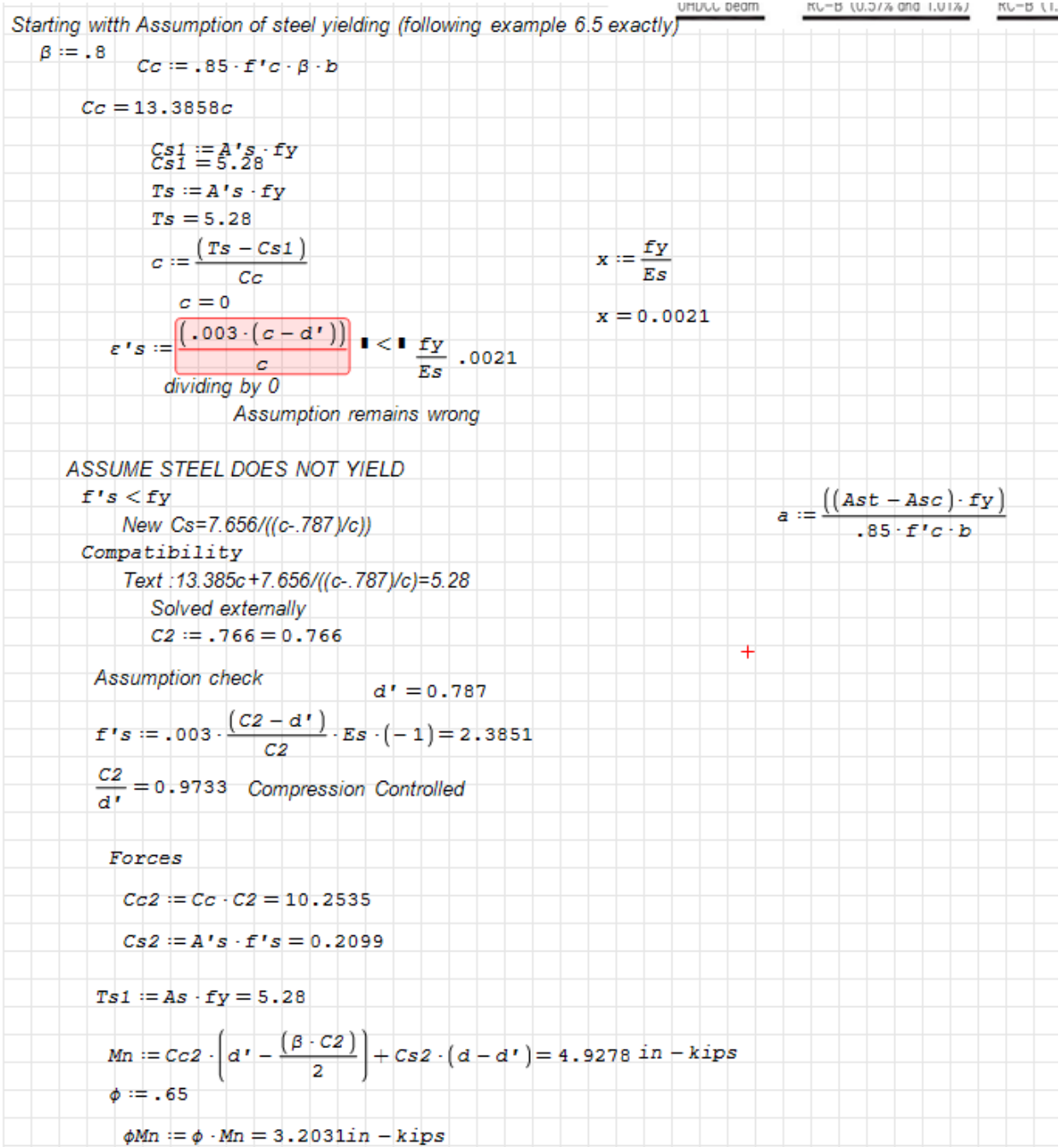


Figure 29: Moment Capacity Calculations for Rectangular Section

Parametric Study of Altering Max Strains

Using the same method, parametric studies were done in Excel to indicate how altering f_{etc} , the max tensile strain allowable for the material, and f_{ecp} , the max compressive strain allowable for the material, would affect the moment capacity of a beam. The results, shown in Fig. 30, are done for a rectangular section, as existing equations could be used. An effort was made to do similar studies with

different sections, but a lack of available equations prevented this from occurring and priorities shifted back to finite element models to supplement this. The results here indicate, as expected, that increasing the strain values results in higher moment capacities, but that the benefits of this reach a limit shown by the curves gradually levelling off. For design purposes, this would indicate this as a value to maximize in intelligent mixture design, if testing it proved simpler than full scale beam testing.

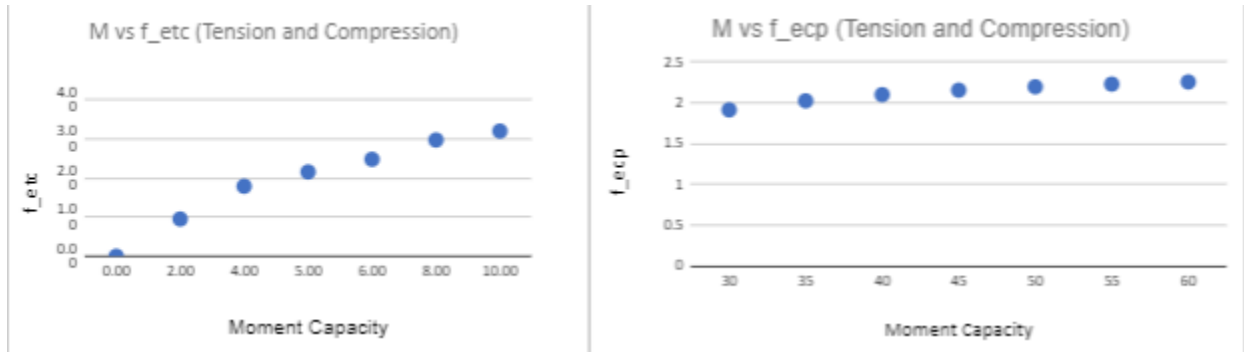


Figure 30: Effect of altering max tensile and compressive strains on Moment Capacity of Unreinforced Square Beam. Note: resultant curves produced the same results in both tension and compression (T &C)

Comparison of Standard Cross Sections

While the above analyses are useful, they are specific to rectangular cross sections that are not likely to be most effective in production. Attempts were made at first to apply the same methods above to more complicated shape factors to generate data for other types of standard beams, such as I sections and trapezoidal ones. However, few examples of this existed, especially for unreinforced sections. As a result, finite element models were adapted to compare stresses across different sections under the same loading conditions. Fig. 31 shows an example of this analysis for several sections. The highlighted section shows that the square beam carries the least tensile load of all the sections. While an optimized AASHTO type section (not pictured) carries the least amount of tensile load for its mass. It is similar to the earlier two sections with a reduced Web thickness and optimize flange dimensions. In addition to printing max tension and compression loads, plots were generated to show variation in stresses throughout the cross section.

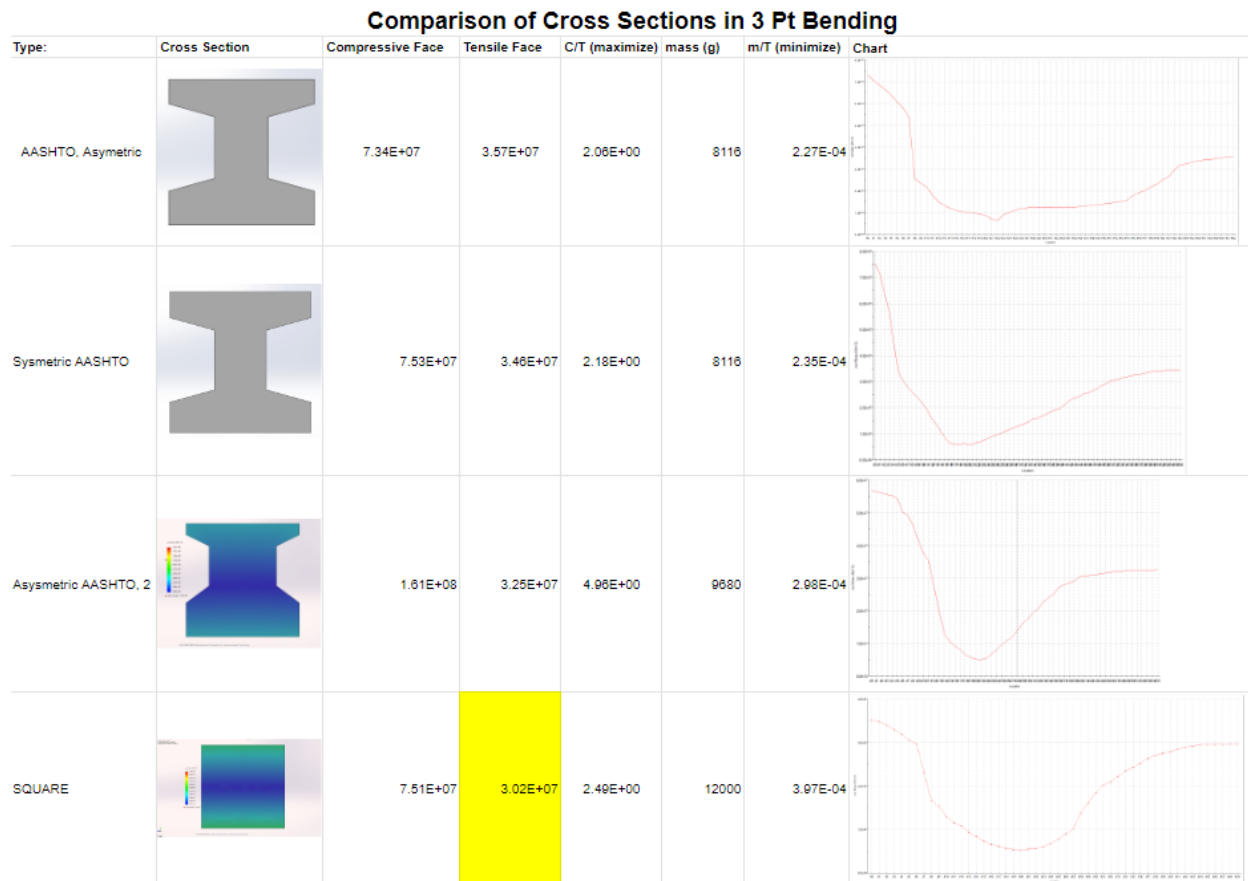


Figure 31: Cross Section Comparison

Finite Element Analysis of ECC

While data for our mixtures of ECC was not complete, using existing data from a series of studies, the set of material properties shown in Table 9 were developed for ECC and used in conjunction with the models created for Fig. 31 above.

Table 9: Material Properties of Analysis and their Sources		
Property:	Value:	Source:
Elastic Modulus (GPa)	32.95	(Yuan et al., 2014)
Shear Modulus (GPa)	21	(Yin et al., 2019)
Tensile Strength (MPa)	4.67	(Abbas et al., 2016)
Compressive Strength (MPa)	49.67	(Abbas et al., 2016)
Yield Strength (MPa)	3	(Yuan et al., 2014)

The two best sections from the comparison, the square and an AASHTO type section, were then analyzed with this new material data. However, in this case, loads were varied and stress was compared by hand with the failure criteria found in literature. In both cases, the models fail due to cracking on the tensile faces in accordance with the material properties defined by Yuan, et al. (Yuan et al., 2014). The square section fails with an unfactored load of 5500 N whereas the AASHTO type fails due to a 3700 N, as shown in Fig 32.

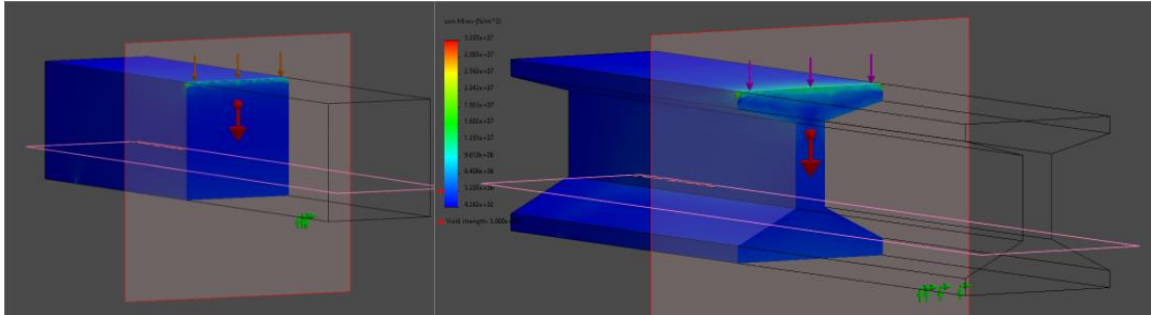


Figure 32: Stress Analysis of Square and AASHTO Type Sections

Printability Modeling

Despite all the effort that has been made, predictions from element models, MathCAD, and matrix methods neglect two important factors that dramatically affect the feasibility of a 3D printed unreinforced beam. The first is the printability of designs. Standard I section, for example, include overhung sections that could not be printed realistically. In addition, the printing process not only introduces geometric stress concentrations due to the layering of material, but also presents its own effects on material properties depending on how the extrusion process occurs. In an effort to model some parts of this, the early-stage model in Fig. 33 was developed. The individual cylinders that make up this model can be altered to reflect the printing parameters used. This should give some graphical idea of what a printed section might look like, and there is a possibility of analyzing this model using similar methods to prior models to give some indication of how the beam will actually perform. However, this would need to be supplemented with data for the printed concrete mixture.

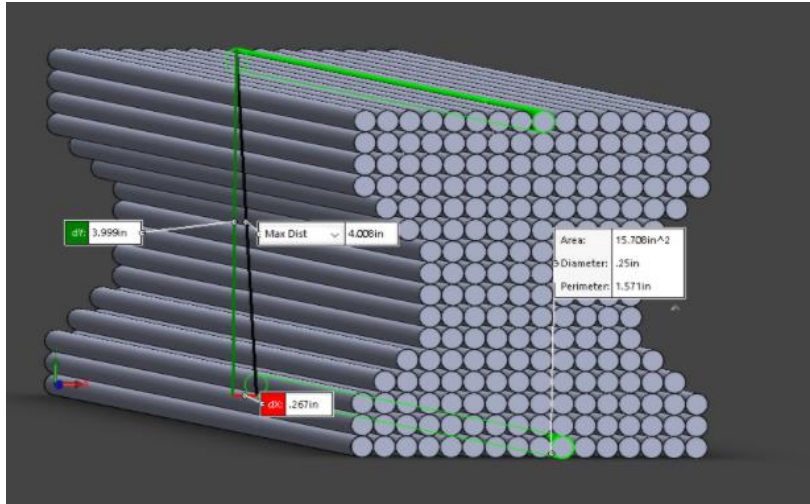


Figure 33: Early-stage printability model

Solidworks Topology Optimization

Additional studies were performed in Solidworks with the beam models that had been generated throughout the fall semester. Rather than simply testing different common beam types, this instead computed a solution based on given parameters. Inputs allowed for a goal to be set of giving the best stiffness to weight ratio (which remains the entire goal of all these analysis methods), as well as an amount of mass to reduce in percent and geometric constraints. This analysis takes a fair amount of computation time, and can result in useless, unrealistic results.

However, with tuning, models like that shown in Fig. 34 can be generated, which are manufacturable at small scale in plastics. In concrete however, the same idea as what is shown here, requires additional post processing to create printable models that remove mass in similar ways.

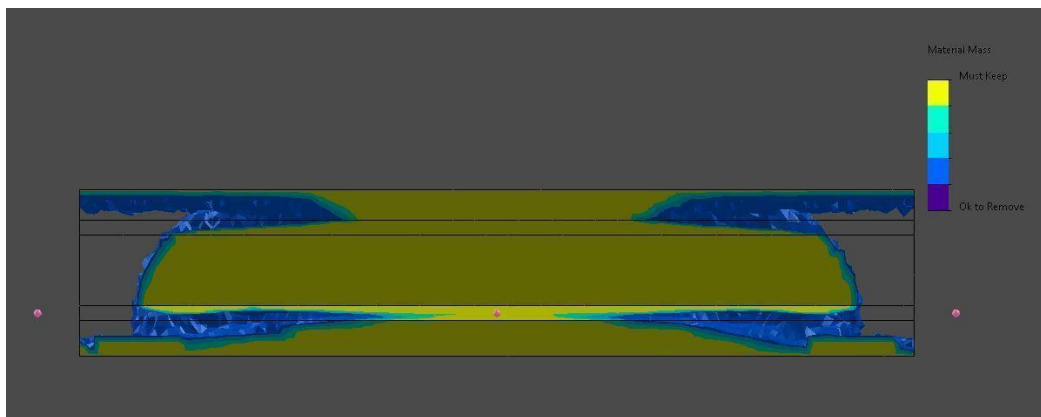


Figure 34: Result of Beam Topology Optimization

While all studies up to this point had used the same beam dimensions as the first replicated beam study, a desire to print beams similar in size to ones able to be cast by existing molds, necessitated switching these dimensions. Thus, models of 3x1.5x12 (in) beams are being created with similar geometry to those in the studies that have been completed.

In addition, 2 types of preparations are necessary to ensure the beams are printable. First, it must be ensured that the geometry is able to be feasibly printable and, second, that data is properly transferred to the printing machine. The first of these considerations was known throughout the design process and resulted in the AASHTO girder inspired beam geometry shown throughout studies. G Code, however, was an unforeseen challenge that is being addressed with simulations like Fig. 35, so that all beams can be printed. Moreover, having a better handle on GCode may allow additional scope to the project, such as tool path comparison.

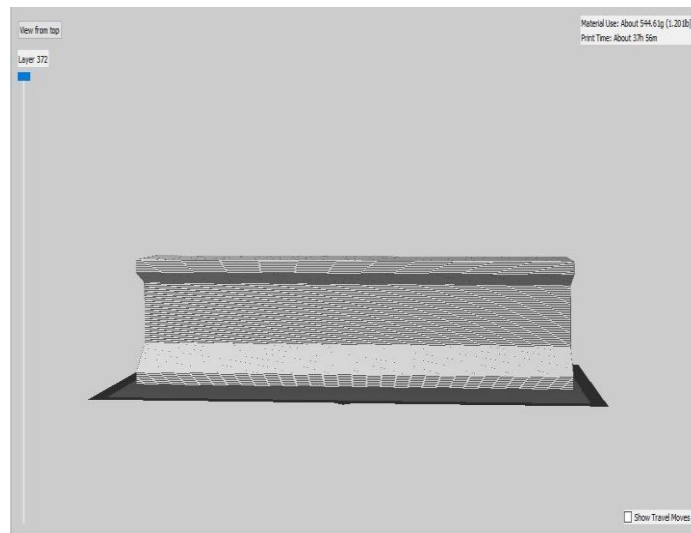


Figure 35: Gcode Simulation of Beam

Final Design Preparation

Factoring in all considerations above, as well as schedule constraints imposed by concrete's curing time and the compressed schedule of this semester, printed beams will not be as developed as originally planned. However, there is opportunity to still obtain valuable design data with simpler printed beam designs. Moreover, the opportunity exists to obtain additional data based on comparison of different printing toolpaths, which may lead to a drastically different mechanical performance.

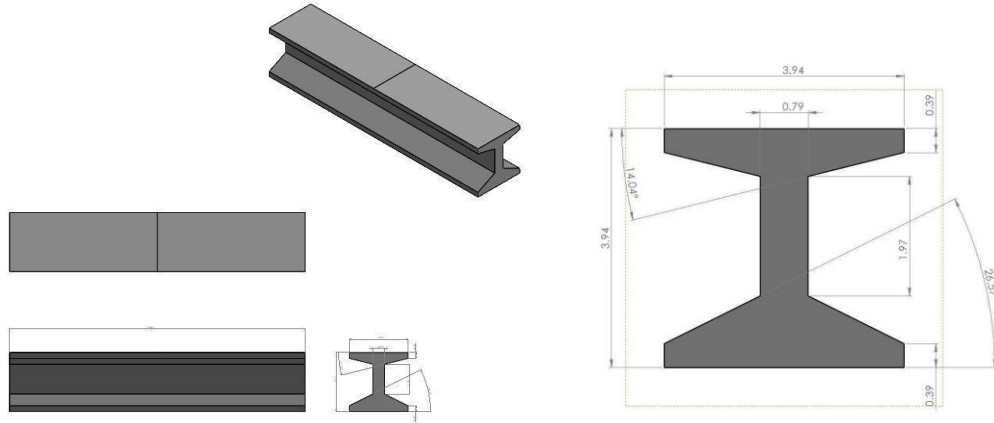


Figure 36: Draft of Finalized Beam Design

Future Work

Challenges presented by a compressed timeline and unexpected complications in the printing process limited the relevance of optimized beam geometry to the project, and resulted in a shift of the ultimate goals of the project. The initial project scope would have allowed more beam designs to be produced, with the ultimate goal of designing an optimized beam that can be practically created with additive manufacturing. Such a beam would be an example of how future structures might use the advantages of 3D printing and fiber reinforced concrete to create future structures that are more mass efficient. Even though the complete development of an optimized geometry was not possible in time allocated, the initial computational geometric studies performed during this project are a good first step and provide useful insights for any future work that aims to print optimized concrete beams.

Such future efforts, therefore, would take the mixture design data generated here and refine it slightly to both increase strength and printability. More critically, however, they would place more focus on refining the printing process to achieve a more consistent print and reduce the stress concentrators located within the beams. Mixtures with different rheological properties could be tested in an attempt to improve the printing characteristics. Furthermore, the use of a larger nozzle could help to reduce any fiber clogging and produce a more uniform printed layer, as well as open up the possibility of printing with larger fiber percentages. The challenge of generating printable GCode was an unexpected one and significant improvement in the project could be made with a more advanced 3D printer capable of accepting GCode generated by software rather than requiring manually written code. Manually generating advanced geometries would be nearly impossible and for that reason was not done. Further development of the printing technology itself and optimal settings are other avenues for further development, as refining the printer settings like feed rate of the printer axes or the extrusion rate of the concrete from the nozzle could greatly improve the quality of printed cross sections if they were studied separately.

Moreover, both testing and design done throughout this project has been limited to flexural members. While the cementitious mixture is transferable to other testing types, the design and printing challenges, as well as the mechanical testing efforts would be completely different for other mechanical

tests, such as compression testing. Efforts by a future team might take a similar approach to that done here, but instead focus on compression members to understand, not only the compressive strength characteristics of the fiber reinforced concrete, but also the challenges of printing tall columnar structures rather than beams. Optimization here may prove less difficult in practice, as the needs for difficult to manufacture cutouts may decrease. Such a project would greatly benefit from developments in mixture design, as well as the challenges seen in translating optimized geometry into production.

Conclusions

During the course of this study, several important questions were able to be answered about the flexural strength of fiber reinforced cementitious composites. The fibers were confirmed to be a valid method of reinforcement, as the flexural strength increased when PVA fibers were added to traditionally cast mixtures. The effects of toolpath on the strength were assessed and it was found that printing in the direction of the tensile load increases strength, due to a greater bonding and fiber alignment. The AM printing process in the optimal toolpath and the cast specimens with fibers were found to have comparable flexural strengths, due to the contrasting effects of reduced cross-sectional area due to the poor interlayer bonding and greater fiber alignment in the AM specimens. Furthermore, the stress distribution and elastic modulus were modeled and predicted for both cast and AM specimens, by a finite element analysis. These promising results suggest, not only that fiber reinforced concrete could be used to supplement rebar reinforcement in low load cases, but also that additively manufactured reinforced concrete can be produced without significant reductions in strength. With further development, this can be refined to improve the printing process for better adhesion between layers and produce less crude products. Significant development is needed before any large structure is built using this technology, but the technology is promising and could be used in the near future.

Furthermore, the topic of geometry optimization and weight reduction was explored. Given the compressed timeframe and occasionally limited resources available, the full extent of this part of the project could not be realized, yet valuable insights and useful data were generated. The greatest example of this is the large amount of time spent developing optimized beam geometry that was ultimately not created in the lab or tested. One might find it difficult to understand how this is related directly to the data generated in the end, but it is important to remember the reasons 3D printing is such an attractive manufacturing method in construction. In addition to schedule and cost savings, 3D printing also allows for irregular, specialized geometries that can be specialized per structure to reduce cost, mass, and construction time. There are other challenges that these methods face, such as regulation, which become further complicated with specialized geometries. The data generated by this team, however, provides valuable insights and suggests that additively manufactured fiber reinforced concretes are indeed feasible. The methods used in this study can be further refined to improve the printing process and coupled with the initial geometric models to generate optimized geometries for use in the construction industry.

Acknowledgements

The Capstone team members would like to thank Ugur Kilic for all his help and guidance with refining the mix design and conducting the rheological and buildability testing. Additionally, we are grateful to Sebring Alden Smith of Lacy Hall, who provided guidance on the specifications of the cast molds and conducted the machining.

References:

- Abbas, M., Taha, M., & Ifrahim, M. S. (2016). *Engineered Cementitious Composites (ECC)*. <https://www.slideshare.net/MuhammadSaadKhan12/engineered-cementitious-composites>
- Audibert, C., Chaves-jacob, J., Linares, J., & Lopez, Q. (2018). Bio-inspired method based on bone architecture to optimize the structure of mechanical workpieces. *Materials Design*, 33(0), 1–16.
- Bhardwaj, A., Jones, S. Z., Kalantar, N., Pei, Z., Vickers, J., Wangler, T., Zavattieri, P., & Zou, N. (2019). Additive Manufacturing Processes for Infrastructure Construction: A Review. *Journal of Manufacturing Science and Engineering*, 141(9), 1–13. <https://doi.org/10.1115/1.4044106>
- Figueiredo, S. C., Romero Rodríguez, C., Ahmed, Z. Y., Bos, D. H., Xu, Y., Salet, T. M., Çopuroğlu, O., Schlangen, E., & Bos, F. P. (2019). An approach to develop printable strain hardening cementitious composites. *Materials and Design*, 169. <https://doi.org/10.1016/j.matdes.2019.107651>
- Hambach, M., & Volkmer, D. (2017). Properties of 3D-printed fiber-reinforced Portland cement paste. *Cement and Concrete Composites*, 79, 62–70. <https://doi.org/10.1016/j.cemconcomp.2017.02.001>
- Ivanova, I., & Mechtcherine, V. (2020). Possibilities and challenges of constant shear rate test for evaluation of structural build-up rate of cementitious materials. *Cement and Concrete Research*, 130(January), 105974. <https://doi.org/10.1016/j.cemconres.2020.105974>
- Lab, R. (2007). Think Formwork - Reduce Costs. *Structure Magazine*, April, 14–16. <http://www.structurearchives.org/article.aspx?articleID=423>
- Li, V. C. (2008). Engineered cementitious composite (ecc): Material, structural, and durability performance. *Concrete Construction Engineering Handbook, Second Edition*, 1001–1048.
- Lu, B., Weng, Y., Li, M., Qian, Y., Leong, K. F., Tan, M. J., & Qian, S. (2019). A systematical review of 3D printable cementitious materials. *Construction and Building Materials*, 207, 477–490. <https://doi.org/10.1016/j.conbuildmat.2019.02.144>
- O’Neal, B. (2016). *The Landscape House Now Underway, 3D Printed by Massive Free-Form Robotic 3D Builder*. 3DPrint.Com. <https://3dprint.com/138208/landscape-house-bam-3d-printer/>
- Schulte, J. M., Kilic, U., Ma, J., & Ozbulut, O. E. (2021). *Rheological and buildability characterization of PVA fiber-reinforced cementitious composites for additive construction*. *March*, 23. <https://doi.org/10.1117/12.2588770>
- Soltan, D. G., & Li, V. C. (2018). A self-reinforced cementitious composite for building-scale 3D printing. *Cement and Concrete Composites*, 90, 1–13. <https://doi.org/10.1016/j.cemconcomp.2018.03.017>
- Starr, M. (2016). *Dubai unveils world’s first 3D-printed office building*. Cnet.Com. <https://www.cnet.com/news/dubai-unveils-worlds-first-3d-printed-office-building/>
- Yin, L., Liu, S., Yan, C., Zhang, J., & Wang, X. (2019). Shear load-displacement curves of PVA fiber-reinforced engineered cementitious composite expansion joints in steel bridges. *Applied Sciences (Switzerland)*, 9(24). <https://doi.org/10.3390/app9245275>
- Yu, K., Li, L., Yu, J., Xiao, J., Ye, J., & Wang, Y. (2018). Feasibility of using ultra-high ductility cementitious composites for concrete structures without steel rebar. *Engineering Structures*, 170(May), 11–20. <https://doi.org/10.1016/j.engstruct.2018.05.037>
- Yuan, F., Pan, J., & Wu, Y. (2014). Numerical study on flexural behaviors of steel reinforced

engineered cementitious composite (ECC) and ECC/concrete composite beams. *Science China Technological Sciences*, 57(3), 637–645. <https://doi.org/10.1007/s11431-014-5478-4>

Zhu, B., Pan, J., Nematollahi, B., Zhou, Z., Zhang, Y., & Sanjayan, J. (2019). Development of 3D printable engineered cementitious composites with ultra-high tensile ductility for digital construction. *Materials and Design*, 181, 108088. <https://doi.org/10.1016/j.matdes.2019.108088>